The Geological Society of America
Special Paper 494
2013

New perspectives on the geometry of the Albuquerque Basin, Rio Grande rift, New Mexico: Insights from geophysical models of rift-fill thickness

V.J.S. Grauch*
U.S. Geological Survey, MS 964, Federal Center, Denver, Colorado 80225, USA

Sean D. Connell†
New Mexico Bureau of Geology and Mineral Resources–Albuquerque Office, New Mexico Institute of Mining and Technology, 2808 Central Ave. SE, Albuquerque, New Mexico 87106, USA

ABSTRACT

Discrepancies among previous models of the geometry of the Albuquerque Basin motivated us to develop a new model using a comprehensive approach. Capitalizing on a natural separation between the densities of mainly Neogene basin fill (Santa Fe Group) and those of older rocks, we developed a three-dimensional (3D) geophysical model of syn-rift basin-fill thickness that incorporates well data, seismic-reflection data, geologic cross sections, and other geophysical data in a constrained gravity inversion. Although the resulting model does not show structures directly, it elucidates important aspects of basin geometry. The main features are three, 3–5-km-deep, interconnected structural depressions, which increase in size, complexity, and segmentation from north to south: the Santo Domingo, Calabacillas, and Belen subbasins. The increase in segmentation and complexity may reflect a transition of the Rio Grande rift from well-defined structural depressions in the north to multiple, segmented basins within a broader region of crustal extension to the south. The modeled geometry of the subbasins and their connections differs from a widely accepted structural model based primarily on seismic-reflection interpretations. Key elements of the previous model are an east-tilted half-graben block on the north separated from a west-tilted half-graben block on the south by a southwest-trending, scissor-like transfer zone. Instead, we find multiple subbasins with predominantly easterly tilts for much of the Albuquerque Basin, a restricted region of westward tilting in the southwestern part of the basin, and a northwesterly trending antiform dividing subbasins in the center of the basin instead of a major scissor-like transfer zone. The overall eastward tilt indicated by the 3D geophysical model generally conforms to

*E-mail: tien@usgs.gov.
†Current address: Chevron Energy Technology Company, 6001 Bollinger Canyon Road, San Ramon, California 94583-2324, USA; e-mail: seanconnell@chevron.com.

Grauch, V.J.S., and Connell, S.D., 2013, New perspectives on the geometry of the Albuquerque Basin, Rio Grande rift, New Mexico: Insights from geophysical models of rift-fill thickness, *in* Hudson, M.R., and Grauch, V.J.S., eds., New Perspectives on Rio Grande Rift Basins: From Tectonics to Groundwater: Geological Society of America Special Paper 494, p. 427–462, doi:10.1130/2013.2494(16). For permission to copy, contact editing@geosociety.org.

stratal tilts observed for the syn-rift succession, implying a prolonged eastward tilting of the basin during Miocene time. An extensive north-south synform in the central part of the Belen subbasin suggests a possible path for the ancestral Rio Grande during late Miocene or early Pliocene time. Variations in rift-fill thickness correspond to pre-rift structures in several places, suggesting that a better understanding of pre-rift history may shed light on debates about structural inheritance within the rift.

INTRODUCTION

The Albuquerque Basin forms the central part of the Rio Grande rift in New Mexico (inset on Fig. 1), and is one of the largest basins of the rift (Chapin and Cather, 1994). It is home to the Albuquerque–Rio Rancho metropolitan area, which is the largest and fastest-growing urban region in New Mexico (Bartolino and Cole, 2002). The basin is bordered on the north and northeast by the west-tilted Española Basin and late rift–stage volcanic fields. Basins with generally west-tilted half-graben segments lie immediately to the south, such as the Socorro Basin (Fig. 1).

Modeling the structure and geometry of the Albuquerque Basin and associated variations in rift-fill thickness is important not only for understanding the tectonic history of the Rio Grande rift (Cordell, 1978; Brown et al., 1980; Baldridge et al., 1995), but also for developing regional groundwater models (Birch, 1982; Bartolino and Cole, 2002), assessing seismic hazards (Wong et al., 2004), and exploring for energy resources (Russell and Snelson, 1994a; Black, 1999; Johnson et al., 2001). Among several previous models of basin geometry, the most widely cited is a structural model developed primarily from seismic-reflection data (Russell and Snelson, 1990, 1994a, 1994b). This model portrays the Albuquerque Basin as structurally segmented into northern and southern half-graben blocks that are oppositely tilted and separated by a large, scissor-like transfer zone. This basic view of the Albuquerque Basin has persisted in the literature (e.g., Chapin and Cather, 1994; Baldridge et al., 1995; Johnson et al., 2001; Ingersoll, 2001, 2003) and grown to represent an archetype of a segmented continental rift basin (Lambiase and Bosworth, 1995; Faulds and Varga, 1998; Younes and McClay, 2002). Although the Russell-Snelson model is informative about aspects of subsurface structure, major elements of basin geometry are conceptually inconsistent with geomorphic and geologic evidence and conflict with observations from gravity and aeromagnetic data (Connell et al., 1998; Connell and Wells, 1999; Grauch, 1999, 2001; Maldonado et al., 1999; Gillespie, 2002; Connell, 2004).

A better view of the overall structure and geometry of the Albuquerque Basin can be achieved through the integration and joint interpretation of various geological and geophysical data sets, as followed in this study. We model the distribution of relatively low-density upper Cenozoic sediments that occupy the Albuquerque Basin using a three-dimensional (3D) inversion of available gravity data constrained by a wide variety of independent information. The resulting model of rift-fill thickness satisfies well information, allows for variable density, matches new structural cross sections, and is consistent with seismic-reflection data. We use this thickness distribution to delineate major geologic structures and elucidate the geometry of the basin. Our model suggests that the Albuquerque Basin predominantly tilts eastward, with westward tilting restricted to the southwest side, and no large, scissor-like transfer zone. With this new perspective, we identify half grabens and strain-accommodation zones, discuss implications for sedimentation and tectonic history, and point out associations with preexisting structures.

PREVIOUS BASIN MODELS

A wealth of geophysical data and borehole information is available for the Albuquerque Basin that can be used to determine its geometry in the subsurface. Previous basin models relied primarily on gravity data (Cordell, 1976), gravity data constrained by borehole data (Birch, 1982; Fig. 2A), or seismic-reflection data combined with borehole data (Russell and Snelson, 1990, 1994a, 1994b; May and Russell, 1994; Fig. 2B). The widely cited Russell-Snelson model was developed in 1978–1980 as part of an oil and gas exploration program by Shell Oil Company (Russell and Snelson, 1994a). Concepts of the model attributed to Shell seismic data were introduced by Lozinsky (1988, 1989) before its publication by Russell and Snelson in the 1990s. May and Russell (1994) added to the model by estimating rift-fill thickness within the basin from borehole and industry gravity data (Fig. 2B).

Key elements of the Russell-Snelson model (Fig. 2B) are (1) an east-tilted half-graben block on the north and a west-tilted

Figure 1. Generalized geology of the Albuquerque Basin and surrounding area. Geology compiled and modified from New Mexico Bureau of Geology and Mineral Resources (2003), Kelley (1977, 1978), Smith et al. (2001), Connell (2008a, 2008b), Maldonado et al. (2007), and Lozinsky and Tedford (1991). Underlying shaded relief image is from the National Elevation Data Set (U.S. Geological Survey) at 30 m resolution. The Albuquerque Basin boundary is used for reference on subsequent figures. We define this boundary as the general limit of mapped syn-rift sediments (Santa Fe Group) extending between volcanic fields of the Jemez Mountains and Cerros del Rio volcanic field on the north and the physiographic constriction between the Ladron Mountains and Joyita Hills on the south. Cf—Coyote fault; CMf—Cat Mesa fault; GF—Gabaldon fault; HSfz—Hubbell Spring fault zone; LPf—Loma Pelada fault; SFf—Santa Fe fault; SYf—San Ysidro fault; TCfz—Tijeras-Cañoncito fault zone. BB—Black Butte; CO—Colorado; NM—New Mexico; emb.—embayment.

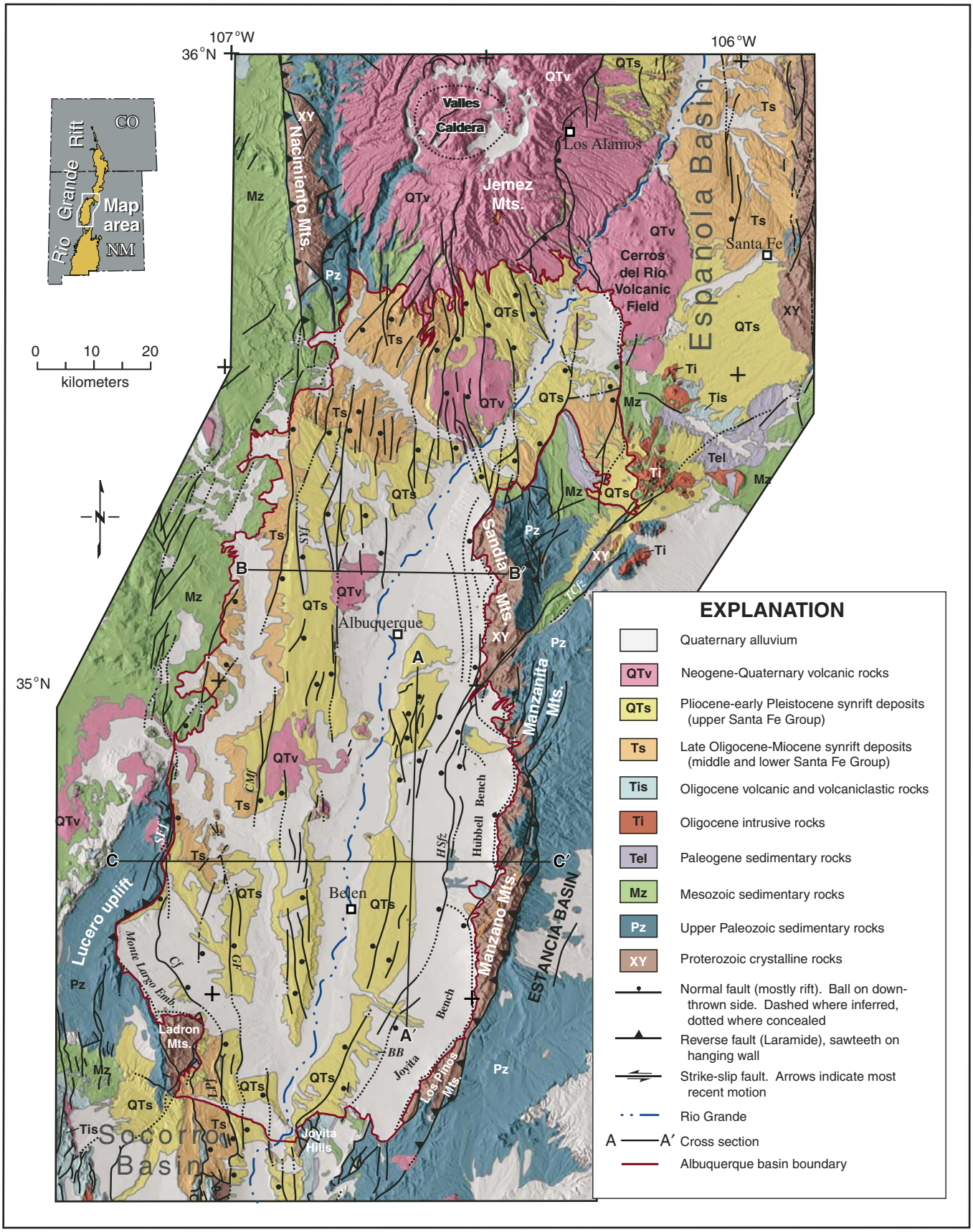

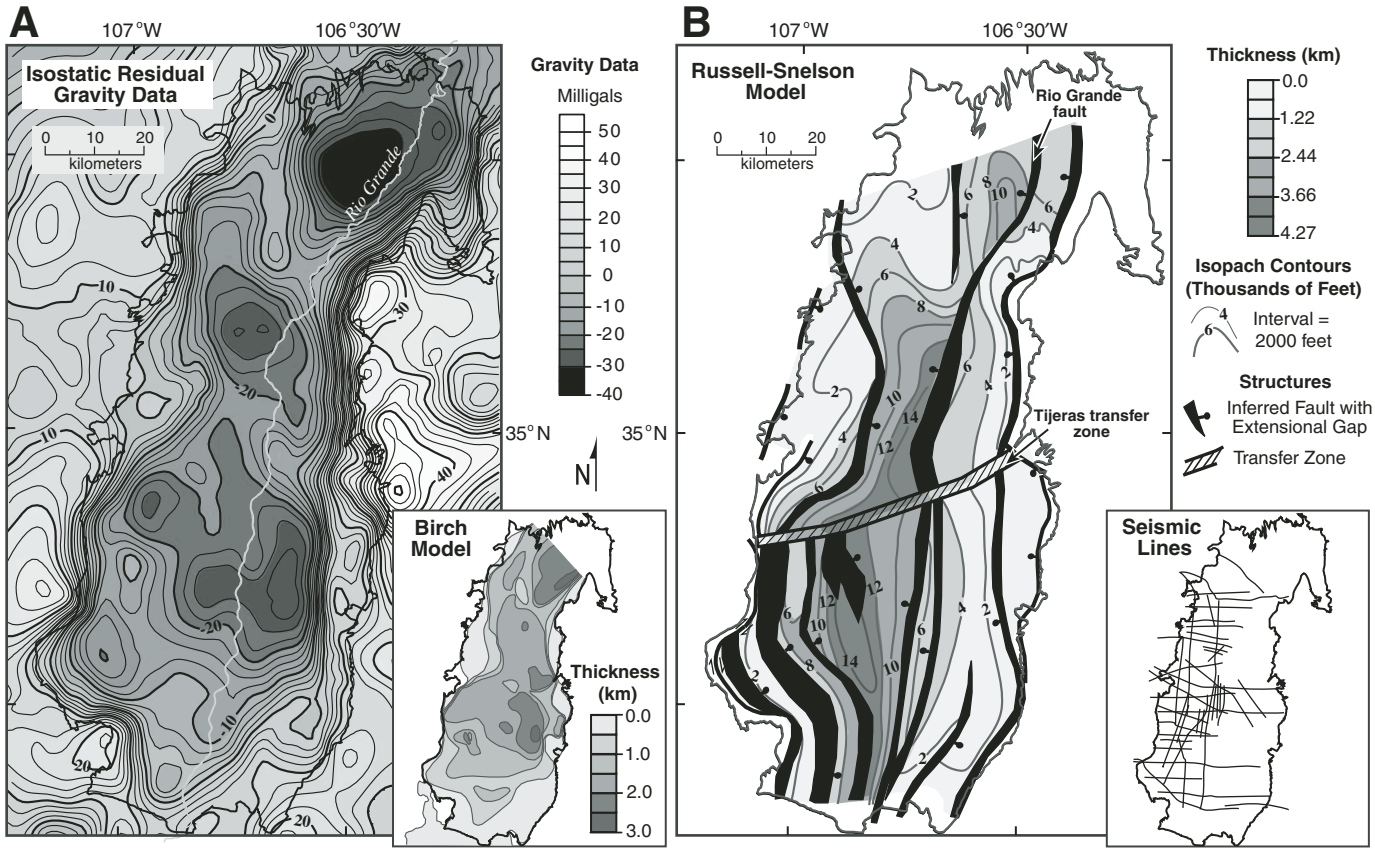

Figure 2. Gravity contour map and two previous basin models. Albuquerque Basin boundary from Figure 1 is used for reference. (A) Isostatic residual gravity data, which are processed to focus on density variations in the upper 10 km of the crust. Inset shows isopach contours of the 2200 kg/m^3 density layer derived by Birch (1982) from profile models, considered to represent Neogene fill (Santa Fe Group). (B) Russell-Snelson model based primarily on well and seismic-reflection data (Russell and Snelson, 1994a) with isopach of Santa Fe Group thickness from May and Russell (1994). Contours are in thousands of feet; the gray scale represents these intervals in kilometers. Note the difference in dynamic range between this gray scale and the one for the Birch model. Inset shows the index map of seismic-reflection lines used by Russell and Snelson (1994a) to construct their structural model.

half-graben block on the south; (2) a southwest-trending transfer zone (their "Tijeras transfer zone") that accommodates the opposing tilts of the north and south half-graben blocks; (3) structural benches along the eastern and northwestern sides of the basin as much as 15 km wide; and (4) a major north-south fault through the middle of the valley (their "Rio Grande fault") that forms the eastern rift border. The "Tijeras transfer zone" is an extension of a long-lived strike-slip fault system that is well documented from the eastern flank of the Albuquerque Basin to the southeastern tip of the Española Basin (TCfz on Fig. 1; Kelley and Northrop, 1975; Abbott et al., 2004; Lisenbee, this volume).

Discrepancies between the Russell-Snelson model and observed gravity data are immediately obvious by comparison with a gravity contour map (Fig. 2). The deepest parts of the rift occur in the middle of the basin in the Russell-Snelson model (Fig. 2B), whereas large gravity lows and the gravity model of Birch (1982) indicate the deepest parts are along the eastern side (Fig. 2A). Large gravity lows are generally associated with depocenters in rift basins (Bott and Hinze, 1995), because of the large contrasts expected between the lower densities of thick sedimentary piles compared to the higher densities of the surrounding and underlying bedrock. This density contrast is especially notable for the Rio Grande rift, because the majority of the fill consists of poorly consolidated Neogene sediments with low bulk densities (Cordell, 1976; Birch, 1982; Cape et al., 1983; Keller et al., 1984). Thus, large gravity lows should be closely associated with thick accumulation of sediment rather than structural benches. Some of these discrepancies may be explained by lack of seismic-reflection data on the east side of the basin where the gravity lows are located (Fig. 2B inset). However, Gillespie (2002) discovered other discrepancies by constructing gravity models from a few of the interpreted seismic sections. These problems suggest that previous geologic interpretations of seismic reflections should be reassessed.

Previous gravity models of the Albuquerque Basin have problems as well. The gravity model by Cordell (1976) was limited by unavailability of borehole data. Borehole constraints are necessary to overcome ambiguities caused by density variations

within the basin floor. Such variations are likely in the rift, arising from variable thickness of the pre-rift sedimentary section and intra-basement density variations (Barrow and Keller, 1994; Grauch et al., 2009). Data from more wells were available for the gravity model developed by Birch (1982), who used an extensive network of 2D profile models and borehole density logs to build a 3D model of Neogene rift-fill thickness (Fig. 2A inset). However, Birch relied on characterizing geologic units on the basis of only three different "density layers." In particular, he equated the layer of lowest density with Neogene fill. The assignment of basin fill to a single density does not allow for density increases with depth due to compaction. As a result, denser layers in his model that should represent deep rift fill may be misidentified as underlying, older geologic units.

Previous interpretations may also have been influenced by problematic stratigraphic picks in some of the older exploration wells. Lozinsky (1988, 1994) used sandstone petrology to resolve the base of rift fill in many of these wells, but one isolated, deep well in the southeastern part of the basin (Grober-Fuqua #1) has been particularly problematic. Alternative stratigraphic picks in this well support the presence of either (1) a structural bench at ~1.4 km depth, or (2) a deeper (>1.9 km) rift basin. Interpretations by most previous workers have supported the structural bench scenario (e.g., Kelley, 1977; Lozinsky, 1994). A more recent reexamination, which highlighted paleomagnetic analysis, lends greater support to the deeper rift basin scenario (Hudson and Grauch, 2003).

Considering the problems and discrepancies among the previous models, we saw the need to develop a new model of rift-fill thickness with a comprehensive approach that (1) reconciles and integrates the seismic and gravity data, and (2) reevaluates the existing and new information with modern interpretation techniques. Because we have access to only a few lines of the Shell seismic data, we must rely primarily on gravity data for modeling. To overcome this limitation, we use a specialized 3D gravity inversion to integrate seismic-reflection and other geophysical data, reduce ambiguity in the model, and avoid problems arising from 2D modeling of 3D structure.

GEOLOGIC AND TECTONIC SETTING

Syn-rift sediments, known as the Santa Fe Group (Spiegel and Baldwin, 1963), were deposited in the Albuquerque Basin during latest Oligocene through early Pleistocene time (QTs and Ts on Fig. 1). The most rapid accumulation occurred during Miocene time (Chapin and Cather, 1994; Connell, 2004). Sediment thickness in boreholes varies from ~1000–2000 m (3280–6560 ft) along basin margins to more than 4270 m (14,000 ft) in basin centers (Lozinsky, 1994; May and Russell, 1994). Upper Oligocene and Miocene sediments of the Santa Fe Group include alluvial, eolian, fluviolacustrine, and volcaniclastic detritus that were deposited within internally drained basins (Chapin and Cather, 1994). In the southern part of the basin, Miocene sediments were deposited in a distal-fan/basin-floor environment, interspersed with ash-flow tuff and basaltic lava flows (Lozinsky and Tedford, 1991).

After local tilting and erosion, the ancestral Rio Grande became organized as a through-going drainage system, depositing fluvial sediments starting by early Pliocene time (Connell, 2004; Connell et al., 2005). Late rift–stage volcanic activity occurred in several isolated centers within the basin (QTv on Fig. 1), mostly along linear vent alignments (Kelley and Kudo, 1978; Crumpler, 1999; Maldonado et al., 2007). More voluminous magmatic activity was located north of the basin in the Jemez Mountains and Cerros del Rio volcanic field (Fig. 1), where volcanic activity may have begun as early as 17 Ma and culminated in caldera formation at ca. 1.2–1.6 Ma (Goff and Gardner, 2004). Contemporaneous sediment accumulation was less than during the Miocene phase of basin subsidence (Lozinsky, 1994; Tedford and Barghoorn, 1999; Connell et al., this volume). Consequently, the Plio-Pleistocene section represents only a fraction of the total volume of rift fill within this basin. This younger basin fill buries much of the older syn-rift deposits, making interpretation of the older history of rifting ambiguous in many places.

In large areas of the Albuquerque Basin, the Santa Fe Group overlies Eocene and Oligocene sedimentary and volcanic rocks and a variably eroded Mesozoic through Paleozoic sedimentary sequence, evidenced in boreholes and recorded in rocks surrounding the basin (e.g., Pazzaglia et al., 1999). Precambrian rocks exposed in the nearby mountains record the earliest tectonic history, notably the Proterozoic accretion of continental material along northeast-trending orogenic belts (Karlstrom et al., 2004). These northeast trends persist as shear zones and thrust belts that many workers consider as controlling structures on subsequent rift formation (e.g., Cordell, 1978; Chapin and Cather, 1994; Karlstrom et al., 1999).

Marine limestone sequences overlain by dominantly shelf and floodplain clastic sediments were deposited unconformably on Precambrian basement from Mississippian through Permian time. The section varied in original thickness from 0.4 to 1.6 km (Kelley, 1977). In late Paleozoic time, north-trending regional uplifts and intervening basins formed in the vicinity of the study area as the result of the Ancestral Rocky Mountain orogeny. Sedimentologic and subsurface evidence suggests that uplifts were coincident with the present-day Nacimiento Mountains and Joyita Hills at the northern and southern ends of the Albuquerque Basin, respectively (Baars, 1982). Associated basins were located on the western side of the Albuquerque Basin and in the Estancia Basin, just east of the Manzano Mountains (Fig. 1; summarized by Pazzaglia et al., 1999). An additional 1.3–2.4 km of marine and nonmarine, mainly siliciclastic, sediments accumulated during Mesozoic time (Kelley, 1977). The Mesozoic–Paleozoic section was structurally disrupted and variably eroded during post-depositional tectonic events. For example, only the basal marine limestone sequence is preserved along the eastern flank of the Albuquerque Basin (Fig. 1).

In Late Cretaceous through Eocene time, the Laramide orogeny formed regional uplifts and intervening basins in the

study area, some of which coincided with the Ancestral Rocky Mountains uplifts. The uplifts occurred as a result of reverse and strike-slip faulting, with accompanying folding (Cather, 2004). Laramide thrust faults, which locally overturned beds, are exposed along the eastern and southwestern sides of the basin (Fig. 1; Kelley, 1977). Rift faults and Laramide structures are superposed along the eastern margin of the Laramide-age Lucero uplift (Fig. 1), forming a complex boundary between the Colorado Plateau and the Rio Grande rift (Kelley and Wood, 1946; Callender and Zilinski, 1976). This structural complexity has sparked debate on whether low-angle and curvilinear faults that project into the southern part of the basin are Laramide thrust faults, Tertiary detachments, or both (de Voogd et al., 1986, 1988; Wu, 1986; Cabezas, 1991; Lewis and Baldridge, 1994). Toward the end of the Laramide orogeny in early Eocene time, detritus shed from regional uplifts collected in basins that were located in the northeastern and southern parts of the present-day Albuquerque Basin (Cather, 2004). Estimated thicknesses range from as much as 1 km in the north to 0.3 km in the south.

Late Eocene–Oligocene eruptions in the northern Socorro Basin (Fig. 1) deposited tuffs and lavas, which probably covered much of the area of the southern part of the basin (Chapin et al., 2004). Because of the wedge-shaped basin geometry next to detachment faults, Cather et al. (1994) considered these rocks to record an onset of weak extension associated with volcanism that preceded deposition of the more sediment-dominated Santa Fe Group. Oligocene intrusions are also located along a north-south belt near the juncture of the Albuquerque and Española Basins (Fig. 1) and may be present at shallow depth ~15 km west of the city of Albuquerque (Grauch, 1999).

Thick accumulations of Oligocene sediments are mainly recognized from boreholes. Called the unit of Isleta #2 by Lozinsky (1994), they range from 485 to 2185 m in thickness. This unit may be correlative to much thinner sections of Oligocene sediments more recently recognized in the northwest part of the Albuquerque Basin and in the southwest Española Basin (Connell et al., 2007; Kelley et al., this volume). Although this unit is not classified as part of the Santa Fe Group, it may record basin subsidence early in rift history (May and Russell, 1994; Connell et al., 2007) rather than passive erosional processes along the northwestern margin of the basin (e.g., Ingersoll, 2001).

The geology of the Albuquerque Basin region records a long tectonic history prior to the initiation of the Rio Grande rift during late Oligocene time. These earlier events left tectonic imprints that can be difficult to distinguish from rift-related features. Superposition of structures is especially confusing. A rare documentation of how subsequent tectonic events have reactivated or superposed their structural signature is presented for the Joyita Hills by Beck and Chapin (1994).

DATA TYPES AND TREATMENT

A variety of geophysical and borehole data were integrated with geologic information for this study. Use of multiple geophysical methods builds on the strengths of each and reduces ambiguity in modeling. Appendix A (available on CD-ROM accompanying this volume and in the GSA Data Repository[1]) provides an overview of the types, strengths, and sources of geophysical data. Appendices B–F (available on CD-ROM accompanying this volume and in the GSA Data Repository [see footnote 1]) provide more detail on specific data types or treatment.

Geophysical Data

Gravity data were compiled for a large region surrounding the Albuquerque Basin so that the gravity inversion would be well constrained (Appendices A and E). Data coverage is fairly good for regional study, but areas lacking stations exceed 10 km in width locally and stations do not adequately cross the basin margins in many places in the south (Fig. 3). Standard Bouguer and terrain corrections were applied using a reduction density of 2670 kg/m^3. In order to focus on density variations within the upper crust, an isostatic regional field was removed from the terrain-corrected Bouguer gravity values, based on parameters established for New Mexico by Heywood (1992). The resulting isostatic residual gravity map (Fig. 2A) generally isolates the gravity effects produced by sources within the upper 10 km of the crust (Simpson et al., 1986). Thus, we assume that only a constant value (as opposed to a trend or smooth regional field as in common practice) need be removed from the data prior to construction of 2D gravity models.

Seismic-reflection data for our study come from two main sources: (1) lines collected by Shell Oil Company (now owned or controlled by Seismic Exchange, Inc.), and (2) lines collected in the mid-1970s as part of the research program Consortium for Continental Reflection Profiling (COCORP) (Brown et al., 1980). Two-way travel time (TWTT) sections for portions of six Shell lines, and time and migrated depth sections from COCORP lines, were available as images scanned from published reports (sources listed in Appendix A). Digital data for four Shell lines (lines 48, 53, 59, and 85; Fig. 3) were purchased and reprocessed by the U.S. Geological Survey (USGS), resulting in migrated depth sections (Appendices B and F). Lines 59 and 85 were not included in the original Russell-Snelson model (inset on Fig. 2B; Russell and Snelson, 1994a). The COCORP data were acquired with five seismic vibrators with a 10–32 Hz sweep and 24-fold stacking, described in more detail by Brown et al. (1980). For the seismic data, we relied primarily on data reprocessing efforts from previous published work (listed in Appendix A) rather than reprocessing the digital data ourselves. de Voogd et al. (1986) explained their processing parameters in detail. In particular, they argued against the use of migration algorithms because they do not work well for lines that cross 3D features.

[1]GSA Data Repository Item 2013199, Appendices A–H, is available at www.geosociety.org/pubs/ft2013.htm, or on request from editing@geosociety.org or Documents Secretary, GSA, P.O. Box 9140, Boulder, CO 80301-9140, USA.

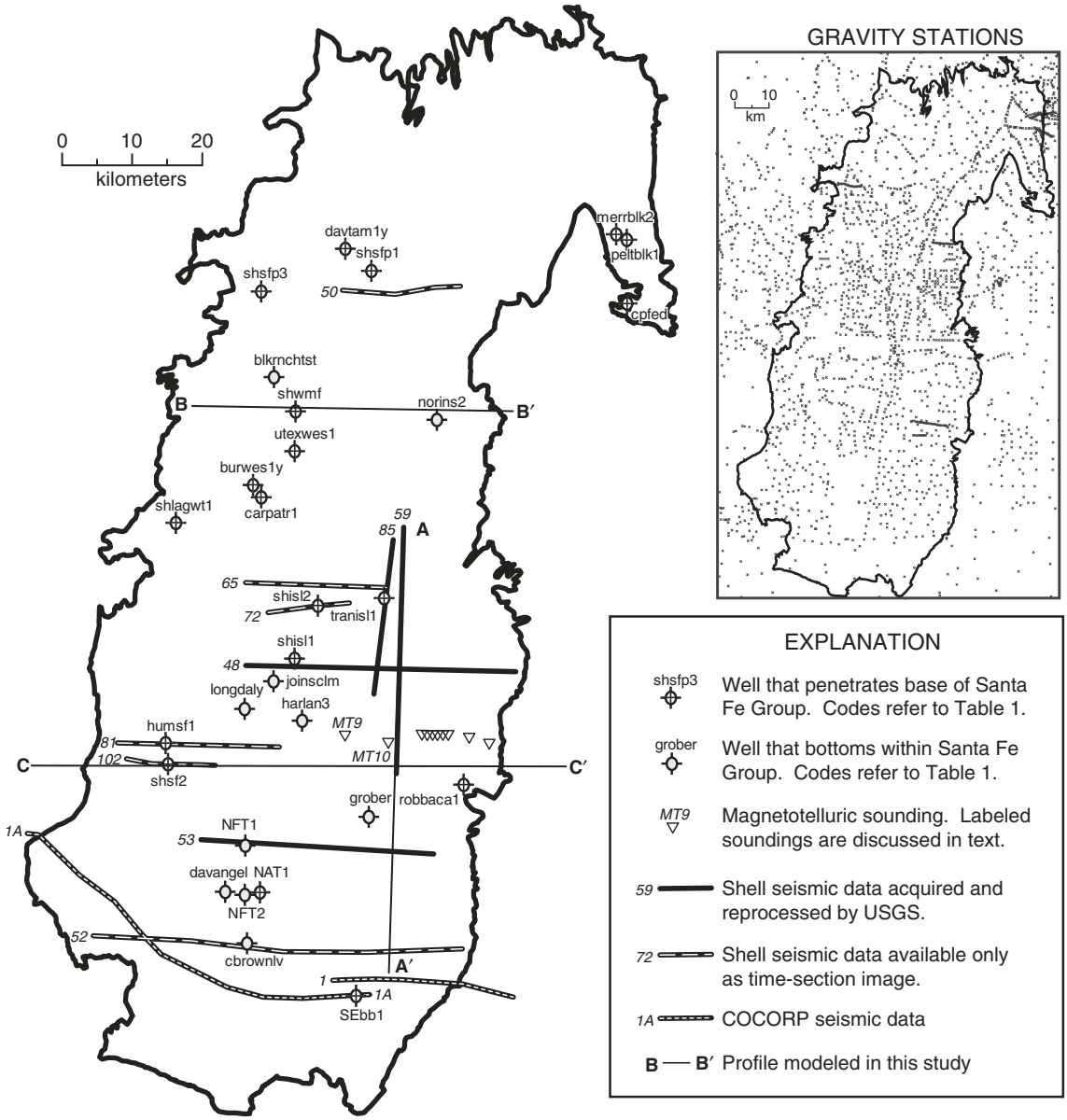

Figure 3. Locations and types of data sources. Basin boundary from Figure 1 is used for reference. Refer to Table 1 for well information and codes. Data sources for gravity, seismic-reflection, and magnetotelluric data are described in Appendices A and B (available on CD-ROM accompanying this volume and in the GSA Data Repository [see footnote 1]). High-resolution aeromagnetic data are presented separately in Appendix C. USGS—U.S. Geological Survey; COCORP—Consortium for Continental Reflection Profiling.

Aeromagnetic data for the study area consist of high-resolution data covering most of the basin (Grauch and Hudson, 2007) merged with regional data compiled by Kucks et al. (2001) for the state of New Mexico (Appendix A). A color shaded-relief image of the reduced-to-pole aeromagnetic data is included in Appendix C. Reduction to pole is routinely applied to correct for asymmetry of anomalies caused by the oblique orientation of the measured magnetic field with respect to Earth's surface (Blakely, 1995). The aeromagnetic data provide several quantitative and qualitative constraints to gravity modeling and seismic interpretation (Appendix F), including constraints on basement features, buried volcanic rocks, and concealed intrabasinal faults. In particular, magnetic depth-estimation methods were applied to the profile data to help locate magnetic basement (Appendix C).

Two-dimensional models from magnetotelluric (MT) soundings available for the study area and neighboring areas to the north are described in Rodriguez and Sawyer (this volume). Data sources are listed in Appendix A. The 2D models image electrical resistivity of the upper 10 km of the crust. Most of the MT constraints are from those used with gravity modeling in the

TABLE 1. WELL DATA USED FOR SANTA FE GROUP THICKNESS IN ALBUQUERQUE BASIN

Site identifier*	Well name	Location†	Surface elevation (m)	Total depth (m)	Interpreted thickness (m)§	Source of Santa Fe Group interpretation#	Sources of alternate interpretations**
Wells that penetrate base of Santa Fe Group							
burwes1y	Burlington Westland 1Y	21-10N-1E	1811	2371	848	Shroba et al. (2003)	N.A.
carpatr1	Carpenter Atrisco #1	28-10N-1E	1766	2028	1006	Shroba et al. (2003)	N.A.
cpfed	Colorado Plateau #1 Federal	35-13N-6E	1908	431	24	Petroleum Information Corp.	N.A.
davtam1y	Davis Petroleum 1-Y Tamara	3-13N-2E	1863	2662	1146	Connell et al. (2007)	Shroba et al. (2003)
humsf1	Humble Shell Santa Fe #1	18-6N-1W	1552	3868	1494	Lozinsky (1994)	N.A.
merrblk2	Merrion Blackshare #2	34-14N-6E	1832	2079	593	Petroleum Information Corp.	N.A.
NAT1	Twinings No. 1 NAT	22-4N-1E	1579	3798	2560	Geophysical logs at NMLSD	N.A.
peltblk1	Pelto Blackshare Federal #1	35-14N-6E	1839	2141	451	Petroleum Information Corp.	N.A.
robbaca1	Robinson C R Baca No. 1	3-5N-4E	1717	719	69	Petroleum Information Corp.	N.A.
shisl1	Shell 1 Isleta	7-7N-2E	1537	4982	2679	Lozinsky (1994)	N.A.
shisl2	Shell 2 Isleta	16-8N-2E	1524	6482	4407	Lozinsky (1994)	N.A.
shlagwt1	Shell 1 Laguna-Wilson Trust	8-9N-1W	1644	3388	3	Petroleum Information Corp.; Black (1999)	N.A.
shsf2	Shell #2 Santa Fe Pacific	29-6N-1W	1583	4360	1460	Lozinsky (1994)	N.A.
shsfp1	Shell #1 Santa Fe Pacific	18-13N-3E	1747	3366	905	Lozinsky (1994)	N.A.
shsfp3	Shell #3 Santa Fe Pacific	28-13N-1E	1917	3132	994	Lozinsky (1994)	N.A.
shwmf	Shell West Mesa Federal	24-11N-1E	1760	1800	2603	Lozinsky (1994)	N.A.
tranisl1	Transocean #1 Isleta	8-8N-3E	1605	3163	1536	Lozinsky (1994)	Discussed in Maldonado et al. (2007)
utexwes1	Utex 1-1J1E Westland Development	1-10N-1E	1760	5080	2493	Shroba et al. (2003)	N.A.
SEbb1	Stellar Energy Black Butte #1	6-2N-3E	1566	1129	155	B. Black (2010, personal commun.)	N.A.
Deep wells that bottom in Santa Fe Group							
blkrnchtst	Black Ranch test well RG-66700-EXPL	3-11N-1E	1804	925	>925	J. Shomaker (1998, personal commun.)	N.A.
cbrownlv	Central New Mexico Brown-Livingston #1	16-3N-1E	1547	866	>866	Black (1982, 1999)	Foster (1978); Lozinsky (1988)
davangel	Davis Angel Eyes #1	19-4N-1E	1476	2461	>2461	Petroleum Information Corp.; Broadhead (2009)	N.A.
grober	Grober-Fuqua #1	19-5N-3E	1531	1920	>1920	Hudson and Grauch (2003)	Discussed in Hudson and Grauch (2003)
harlan3	Harlan Ranch #3	5-6N-2E	1475	1973	>1973	B. Brister (2003, personal commun. reported in Maldonado et al., 2007)	Kelley (1977)
joinsclm	Joiner San Clemente #1	23-7N-1E	1581	1709	>1709	Lozinsky (1994)	N.A.
longdaly	Long Dalies #1	32-7N-1E	1856	2589	>2589	Foster (1978)	Petroleum Information Corp. data reported in Maldonado et al. (2007)
norins2	Norins Realty North Albuquerque Acres #2	19-11N-4E	1640	1531	>1531	Lozinsky (1988)	N.A.
NFT1	Twinings No. 1 NFT	33-5N-1E	1583	2268	>2268	Petroleum Information Corp.; Broadhead (2009)	N.A.
NFT2	Twinings No. 2 NFT	28-4N-1E	1558	2792	>2792	Petroleum Information Corp.; Broadhead (2009)	N.A.

Note: This list does not include the wells and constraint points from magnetotelluric models and seismic-reflection data used outside the study area in the Española Basin region. See Grauch et al. (2009) for a listing of those points.

*Site identifier refers to Fig. 3.

†Location—section-township-range.

§Interpreted thickness involves picking the base of Santa Fe Group in the well or determining whether the base is penetrated at all.

#NMLSD—New Mexico Library of Subsurface Data, New Mexico Bureau of Geology and Mineral Resources.

**Sources that present alternate interpretations are listed only where disagreements were resolved during the course of this study. N.A.—not applicable.

Española Basin (Grauch et al., 2009). The Hubbell Spring MT model, located ~5 km north of profile C–C′ (Fig. 3), shows a deep resistor below a variably conductive section (Rodriguez and Sawyer, this volume). The MT model is useful for estimating the general depth to the resistive, limestone-dominated base of the Paleozoic section.

Borehole Data

A variety of data from exploration and water wells were used to (1) constrain rift-fill thickness in the gravity inversion and check the results, (2) guide construction of geologic cross sections and geophysical profile models, and (3) develop density-depth functions for different geologic units (discussed in the next section). Constraints and checks on rift-fill thickness were provided by 29 oil-exploration wells in the Albuquerque Basin (Fig. 3; Table 1) and from wells of mixed type, MT, and seismic-reflection data at 108 sites in the Española Basin, north and east of the Albuquerque Basin. The large number of constraints for the Española Basin comes from a similar 3D modeling study for that basin (Grauch et al., 2009), thus providing easily accessible regional constraints for this study and ensuring compatibility between the studies.

The presence or absence of the basal contact of the Santa Fe Group in many of the wells has been the subject of controversy. Because these determinations are critical for the gravity inversion, we have resolved them to the best of our ability (Table 1). Additional shallow water and exploration wells (total depths <900 m) were available for construction of geologic cross sections and development of stratigraphic concepts in the northern part of the Albuquerque Basin; these data are available from Connell (2006).

Density Characterization

Gravity modeling that isolates the effects of rift fill from other effects is predicated on a large contrast between densities of the rift fill with those of the surrounding and underlying bedrock. To investigate this contrast for our study, we used borehole density logs from 38 wells to characterize the variation of density with depth for geologic units grouped by age and rock type (Appendix D). Densities for rocks from each category were averaged over equal depth intervals and then simplified into simple, step-like density-depth functions so that they could be easily used in the 2D and 3D modeling. Because each age range consists predominantly of similar rock types, the results show a first-order variation in density by age (Fig. 4).

The resulting, highly averaged, step-like density-depth functions for each age range show that densities of the basin fill (Santa Fe Group, including interbedded volcanic rocks) are systematically much lower (≥400 kg/m^3 difference) than those of the older units at comparable depths to at least 4.25 km (Fig. 4). This systematic difference allows gravity modeling and inversion to robustly separate the gravity effects of the Santa Fe Group from those of the older units throughout much of the basin. Only the density-depth function derived for the Santa Fe Group is necessary for the 3D gravity inversion (Table 2). Although multiple or more complicated density-depth functions could be constructed from the well data, we have found the one in Table 2 to give good results in comparison to independent information in a wide range of situations and in a variety of model tests. High-density volcanic rocks contained within the rift fill appear to locally increase the densities of the Santa Fe Group in the vicinity of isolated volcanic fields. However, the effects are difficult to quantify, so they are evaluated qualitatively, as described below under Model Limitations and explained in more detail in Appendix E.

The derived density-depth functions for all the groups of geologic units were used to construct polygonal bodies and assign densities in the 2D gravity models. Moreover, the functions provide a rationale for combining geologic units into broad categories on the basis of density. For example, the similarity of density-depth functions for Paleogene and Mesozoic units argues for grouping them as a single model unit in the 2D gravity models. Moreover, pre–Santa Fe sedimentary units cannot be distinguished on the basis of density below 3.25 km depth—a limitation

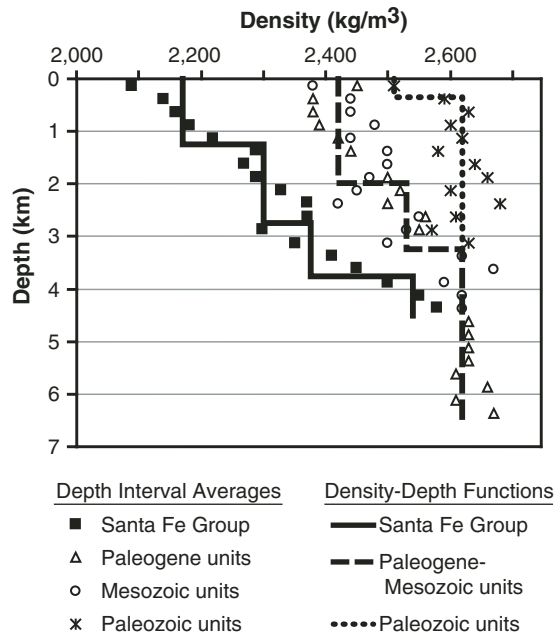

Figure 4. Density-depth characterization of sedimentary groups by age. For each group, densities derived from borehole density logs from 38 wells are averaged at 250 m depth intervals. The data were generalized even further into simple density-depth step functions to use in two-dimensional (2D) and three-dimensional (3D) models. The density compilation is described in more detail in Appendix D (available on CD-ROM accompanying this volume and in the GSA Data Repository [see footnote 1]). A natural separation in density is apparent between Santa Fe Group (syn-rift deposits) and older units to depths of ~4.25 km.

TABLE 2. DENSITY AND VELOCITY FUNCTIONS USED FOR THE SANTA FE GROUP

Depth range (km)	Bulk density (kg/m^3)	Two-way travel time interval (seconds)	Seismic velocity (km/s)
<1.25	2170	<1.19	2.1*
1.25–2.75	2300	1.19–2.26	2.8*
2.75–3.75	2380	2.26–2.83	3.5†
>3.75	2540	>2.83	4.5†

Note: For modeling, densities are assigned to the Santa Fe Group for the depth ranges indicated (also plotted in Fig. 4). To compare Santa Fe Group reflections on seismic time sections to depth models, time is converted to depth using the indicated velocities and time intervals. Depth is converted to time conversely. Time intervals are equivalent to the depth ranges for convenience.

*Taken from velocity analyses by Jurdy and Brocher (1980) and Brocher (1981) for the Consortium for Continental Reflection Profiling (COCORP) seismic data from the southern Albuquerque Basin.

†Computed from the density column using the empirical relation of Gardner et al. (1974).

that prevents resolution of any deep pre-rift structures in the 2D gravity models without the help of other information.

Depth-Time Conversion

Owing to the difficulty of directly comparing model results (in depth) to seismic-reflection profiles available only as scanned images of time sections, it was necessary to apply a simple depth-time conversion to the Santa Fe Group. To do this, we determined seismic velocities for the Santa Fe Group that could be applied over the same depth ranges as defined by the density-depth function (Table 2). The velocities we chose rely on seismic-refraction studies that used first arrivals on shot gathers from the COCORP seismic-reflection survey (Jurdy and Brocher, 1980; Brocher, 1981) and empirical relations of density to velocity in sedimentary basins (Gardner et al., 1974). The velocity of 2.1 km/s for depths <1.25 km is also consistent with compressional velocities measured in sonic logs from wells in the southern Albuquerque Basin (Brown et al., 1980; Brocher, 1981; Cape et al., 1983).

Model depths at specific locations are converted to TWTT using the appropriate velocities over the depth ranges indicated. Conversely, points digitized from reflections on time sections are converted to depth by applying the appropriate velocities over the TWTT intervals indicated. In this way, we can compare model results directly to time sections, establish constraints for the gravity inversion, and determine stratal tilts from reflections. This depth-time conversion was not applicable to the reprocessed seismic-reflection data, which were converted to depth using more sophisticated, digital analyses (Appendix B).

MODEL DEVELOPMENT

The basis of our model development is a 3D gravity inversion designed specifically for modeling basin-fill thickness onto which we iteratively apply constraints from geologic mapping and borehole, seismic-reflection, aeromagnetic, and MT information. Specifically, the inversion (1) incorporates known density information, (2) satisfies independent geological and geophysical constraints, (3) treats the rift basins separately from the complications of the underlying sedimentary section as much as possible, and (4) accommodates 3D aspects of basin shape. Moreover, we develop the 3D basin model with a "bootstrap" approach by reevaluating seismic interpretations and geologic concepts while validating and adjusting the model to fit these constraints. Bootstrapping ensures that all aspects of the process are internally consistent and allows us to use the model results to evaluate and update the previous work.

We first run the gravity inversion with only the most objective constraints to get an initial 3D gravity model. The gravity inversion is described briefly in the following subsection and in more detail in Appendix E. Next, we evaluate the initial model using detailed 2D geophysical modeling, geologic cross sections, and available seismic sections. Where the initial model generally agrees with previous seismic interpretations for which we do not have data, we gain confidence that we can use these interpretations as constraints. Where the model disagrees, we resolve the differences using our available seismic data and geologic information. Finally, we use the 2D interpretations to constrain a final run of the gravity inversion, resulting in a fully constrained 3D basin model.

Gravity Inversion

We use a gravity inversion technique developed specifically for sedimentary basins by Jachens and Moring (1990), modified to explicitly incorporate local depth constraints, as implemented in computer program DEPTH2BS, version 1.6.8 (B.A. Chuchel, U.S. Geological Survey). The technique is based on separation of observed data into regional and residual components, where the residual component represents the gravity effects of the thickness of basin fill and the regional component represents the effects of density variations in bedrock underlying and adjacent to the basin. Regional/residual field separation has been a long-standing problem in gravity modeling because of its subjectivity (Nabighian et al., 2005). However, in this approach, application of geologic constraints during the inversion forces the separation to be compatible with geologic reasoning, thereby reducing much of the ambiguity.

A regional field for the whole basin is initially constructed using data only from gravity stations located on the bedrock that surrounds the basin and internal basin constraints provided by the user. The initial regional field is subtracted from the observed

data to give a starting approximation of the residual field. The inversion then iteratively adjusts a 3D model of basin-fill thickness (following the method of Bott, 1960) and the regional field until the thicknesses and associated forward gravity models match the observed gravity data and best meet all constraints applied by the user.

Two types of constraints are applied during the gravity inversion: (1) *thickness constraint points,* where the inversion attempts to match known values of rift-fill thickness; and (2) *regional-field constraint points*, where the inversion incorporates fixed values of the regional gravity field into the regional/residual separation. Thickness constraint points provide a direct control on the model. Regional-field constraint points are empirically derived to force the inversion to modify thickness in areas where model results are inconsistent with deep wells that do not reach the base of the Santa Fe Group. These wells cannot be used as direct constraints on thickness, but their total depths provide information on minimum thickness. After evaluation of inversion results, the user can adjust constraints for subsequent inversion runs.

The forward model calculations used to test goodness of fit after each iteration of the inversion rely on user-defined density contrasts assigned to different depth layers and an algorithm based on Fourier transforms (Parker, 1973). Readers are referred to Jachens and Moring (1990), Blakely (1995, p. 231–232), Saltus and Jachens (1995), and Jachens et al. (1996) for more explanation of the technique. Ferguson et al. (1988) presented a similar approach.

Application to Albuquerque Basin

In our application, syn-rift Santa Fe Group is designated as "basin fill" and all older geologic units as "bedrock," a natural separation that arises from the differences in overall densities between these groups at a range of depths (Fig. 4). To aid in characterizing the flanks of the basins as well as their interiors, we expanded the area of analysis to include a large region surrounding the Albuquerque and parts of the Española and Socorro Basins (Fig. 1; Appendix E). In map view, the rift basins are collectively defined by the mapped limit of Neogene units and assigned the density-depth function derived for the Santa Fe Group (Table 2) in preparation for the inversion. Because the Santa Fe Group includes interbedded and overlying volcanic rocks (Fig. 1), the final 3D basin model should be considered as an overall model of the combined sedimentary and volcanic portions of the rift fill.

We began by developing an initial *3D gravity model* using the gravity inversion and minimal constraints (no seismic constraints within the Albuquerque Basin). Thickness constraint points were taken from (1) wells that completely penetrate the Santa Fe Group within the Albuquerque Basin (Table 1), and (2) wells and point locations from geophysical data outside the immediate study area that were vetted previously for the Española and northern Albuquerque Basins (Grauch et al., 2009). Regional-field constraint points were applied in the vicinities of Long-Dalies #1, Davis Angel Eyes #1, and Twinings No. 2 NFT wells (Fig. 3) by inspection. An isopach map of rift-fill thickness derived from the 3D gravity model is shown in Figure 5A. A similar 3D gravity model was developed in this fashion (but with fewer constraints) for groundwater studies (Bartolino and Cole, 2002, p. 40).

To arrive at the final *3D geophysical model*, additional thickness constraint points derived from seismic interpretation were applied in steps, as we assessed all the information and developed 2D geophysical models or reexamined seismic-reflection sections to validate concepts in various critical areas. Details regarding this assessment are discussed for key areas in the Model Validation section below. Two-dimensional geophysical models were constructed using a 2-1/2D modeling algorithm capable of truncating polygonal bodies out of the plane of the section to simulate 3D geometries (Geosoft GM-SYS version 7.1.1 [http://www.geosoft.com/products/gm-sys]). The final 3D geophysical model of rift-fill thickness, after all additional constraints were applied, is shown in Figure 5B. The locations of the constraints are coded by source of information. Errors in the fit of computed and observed gravity fields are near zero over most of the grid area, but are locally 10–15 mgal where data coverage is poor at basin margins. Errors in the fit of modeled to known thickness at constraint points are generally within 5% of the actual thickness. Appendix E provides more detail and discussion of errors in the inversion process.

We constructed a structural elevation grid by subtracting thickness values of the final 3D geophysical model from a smoothed digital terrain model. The terrain is smoothed and regridded (0.5 km interval) to match the resolution of the 3D model so that artifacts of topography are not introduced during the subtraction. Digital grids from the final 3D geophysical model representing rift-fill thickness variations, the structural elevation of the base of the Santa Fe Group, and the smoothed terrain used to construct the structural elevation grid are available from Appendix H (available on CD-ROM accompanying this volume and in the GSA Data Repository [see footnote 1]).

The initial 3D gravity model shows a remarkable similarity in gross shapes of features to the final 3D geophysical model, which has seismic constraints applied (Fig. 5). During model evaluation, we found that the shapes of features of the 3D gravity model mimicked patterns in the seismic data and in independently constructed geologic cross sections, giving confidence that initial inversion parameters had been appropriately chosen. Thus, we use the 3D gravity model in subsequent sections to show what is required or permissible by the gravity data alone. The largest differences after application of the additional constraints are moderation of local excursions that appear geologically unreasonable and better delineation of a ridge in the south-central part of the basin.

The 3D gravity model (Fig. 5A) has only passing resemblance to the earlier gravity model by Birch (1982) (inset on Fig. 2A), who used most of the same gravity and well data that we did. The differences and improvements in our model can be attributed to (1) modeling that is truly done in 3D versus construction of 3D results from 2D models, (2) our use of multiple density layers to represent the Santa Fe Group rather than just

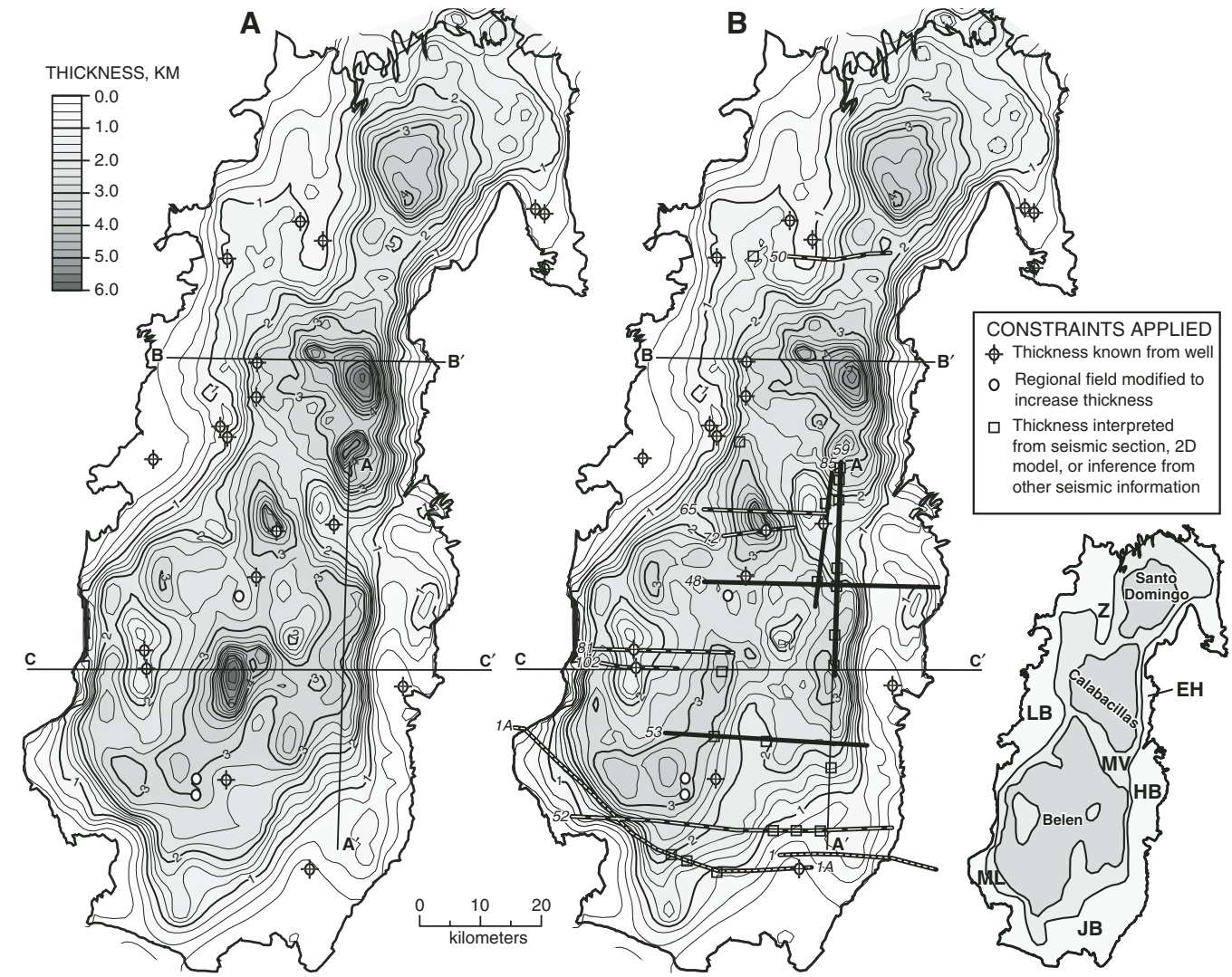

Figure 5. Isopach maps of the three-dimensional (3D) model of rift-fill thickness at initial and final stages of model development. Basin boundary of Figure 1 is shown for reference. The different types of constraint points are explained in text. (A) Isopachs from the initial 3D gravity model that shows what is required or permissible by the gravity data alone. (B) Isopachs from the final 3D geophysical model after all constraints are applied. Seismic lines (coded as in Fig. 3) are shown for reference. Inset shows shaded subbasin areas for reference on this and subsequent figures. The subbasins are generally outlined by the 1 km and 2 km isopach contours of the final 3D geophysical model (B). HB—Hubbell bench; JB—Joyita bench; LB—Laguna bench; ML—Monte Largo embayment; MV—Mountainview prong; EH—East Heights structural bench; Z—Ziana structure.

one, and (3) additional gravity data collected in the southwest part of the basin in 1997 (Gillespie et al., 2000).

Model Limitations

Limitations of the model are described in detail in Appendix E. The most significant of these include (1) local thickness extremities caused by inappropriate regional/residual field separation in the vicinity of abrupt density-contrast boundaries; (2) local excursions of thickness values caused by errors introduced by inadequate gravity data coverage; (3) a tendency to smooth out abrupt thickness variations across normal faults; (4) thicknesses that are in error because assumed density-depth variations are oversimplified; and (5) a tendency to exaggerate thickness trends below high-relief topographic slopes.

A noticeable example of the first limitation is a local thickness extremity of the initial 3D gravity model in the center of the Belen subbasin (Fig. 5A). These types of excursions were mostly remedied by additional seismic constraints, as demonstrated by the diminution of this feature in the final 3D geophysical model (Fig. 5B). In contrast, local excursions caused by inadequate data coverage could not be fixed, and are most noticeable as unreasonably steep gradients at the basin margins, where data coverage is sparse. Smooth rather than abrupt thickness variations across

normal faults arise from the reliance on grids to model thickness. Despite this problem, major basin boundaries are still readily identifiable, albeit somewhat ambiguous regarding dip and presence of a single versus multiple faults. On the other hand, small-offset faults may not be recognizable in the model, and multiple faults may appear as a sloping surface.

Errors in thickness caused by oversimplification of assumed density-depth variations are not conspicuous and difficult to quantify, but are greatest where the rift fill thickness is <100 m (Appendix E). Because the gravity inversion works with density contrast (relative to the reduction density of 2670 kg/m^3), actual densities that are higher or lower than the densities input to the model will result in a modeled basin that is too shallow or too deep, respectively. Higher densities compared to the assumed density-depth function for Santa Fe Group are suspected underneath the volcanic fields, but not modeled separately, as explained in Appendix E. The resulting density "pull-up" of the base of the thickness model is analogous to a velocity pull-up in seismic interpretation, although the physical causes are different. We estimate that large density pull-ups (>10% error in depth) occur where >10%–12% of the top 1.25 km of basin fill is composed of basalt, similar to an estimate given by Drenth et al. (this volume). We also experimented with different density-depth functions for the Santa Fe Group; the one given in Table 2 provided the most reasonable results relative to geologic concepts and trends observed in seismic-reflection sections.

MODEL RESULTS

The fully constrained 3D geophysical model of the Albuquerque Basin (Fig. 5B) captures important aspects of both previous basin models (Fig. 2), but improves on both of them. From the new model, deep parts of the Albuquerque Basin extend much farther east than in previous seismic interpretations, and do not necessarily correspond to the extreme gravity lows. The basin geometry depicted by the model is primarily a reflection of Miocene rift-fill thickness, because Pliocene deposits unconformably overlie Miocene deposits and are relatively thin in comparison.

Figure 6 shows the structural elevation grid of the base of the Santa Fe Group in plan and 3D perspective view. The images represent relief on the rift flanks as well as on the basin floor, so that the rift can be visualized as though the basin fill has been removed. When considering these views, the limitations of the modeling method must be kept in mind. For example, steep gradients can represent one major normal fault or a narrow zone of faults accommodating large vertical displacement; shallow gradients can represent a series of step-down normal faults or a single low-angle fault; and the surface roughness may or may not be significant.

Basin Morphology

The Albuquerque Basin ranges from ~20 km wide in the northern part to ~40 km wide in the southern part. The basin constricts to ~5 km wide at the northern and southern tips, at the connections to the Española and Socorro Basins, respectively. The primary features in both the initial and final 3D models for the Albuquerque Basin are a series of interconnected structural depressions, with intervening structural culminations and flanking structural benches (Fig. 5). The subbasins, which were recognized and named previously (Hawley, 1996; Grauch et al., 1999; Connell, 2004), increase in width and complexity from north to south: the Santo Domingo, Calabacillas, and Belen subbasins. Some workers consider the Santo Domingo subbasin as a unique basin because of its structural setting between the west-tilted Española Basin on the north and the east-tilted northern Albuquerque Basin on the south (e.g., Smith et al., 2001; Minor, 2006). However, we do not model this subbasin separately because it is difficult to distinguish physiographically from the rest of the Albuquerque Basin (Fig. 1; Kelley, 1977; Connell, 2004).

The eastern side of the Albuquerque Basin is bounded by steep slopes in the model, which represent major fault zones of stepped-down blocks with 2–4 km of overall vertical displacement. The steep slopes trend north-south along the east sides of the Calabacillas and Belen subbasins and northeast along the southeast side of the Santo Domingo subbasin. Thick (>3 km) rift fill in these subbasins terminates abruptly against shallow (<1 km) rift fill, represented by steep gradients in isopach contours on Figure 5B. These north-trending terminations generally agree with the geologically determined boundaries of structural benches that are adjacent to the eastern mountain fronts (Black and Hiss, 1974; Kelley, 1977, 1979; Woodward, 1977; Cordell, 1978, 1979). These include a 1–7-km-wide bench called the East Heights fault zone (Connell, 2008b) on the north, and the 8–13-km-wide Hubbell bench on the south (EH and HB on inset, Fig. 5). A broad, northwest-elongated structural high, called the Mountainview prong (Hawley, 1996; Maldonado et al., 1999; Connell, 2004), emanates from the area between the East Heights and Hubbell benches and forms the division between the Calabacillas and Belen subbasins (MV on Fig. 5 inset). The thick basin fill bounded on the east by north-south linear boundaries and northwest-trending Mountainview prong are required by the gravity data, as indicated by the shapes of anomalies in the original gravity data (Fig. 2A; Cordell, 1978) and the initial 3D gravity model (Fig. 5A).

The western border of the Albuquerque Basin is segmented, with a noticeable pattern of en echelon north-south segments at the western sides of all three subbasins, connected by northeast segments representing the southern edges of the Laguna bench and the Ziana structure (Fig. 6). The modeled border has moderate to steep slopes, representing overall 1–2 km of vertical displacement. Where the slope is gentler, the vertical displacement is accommodated across a series of stepped-down faults or locally across low-angle faults. The map pattern of the western border depicted in our model also has been recognized previously (Cordell, 1976, 1978; Kelley, 1977, 1979; Birch, 1982; Russell and Snelson, 1994a; Fig. 2).

The 3D geophysical model depicts the symmetry of the Santo Domingo subbasin within a broader, northeast-elongated

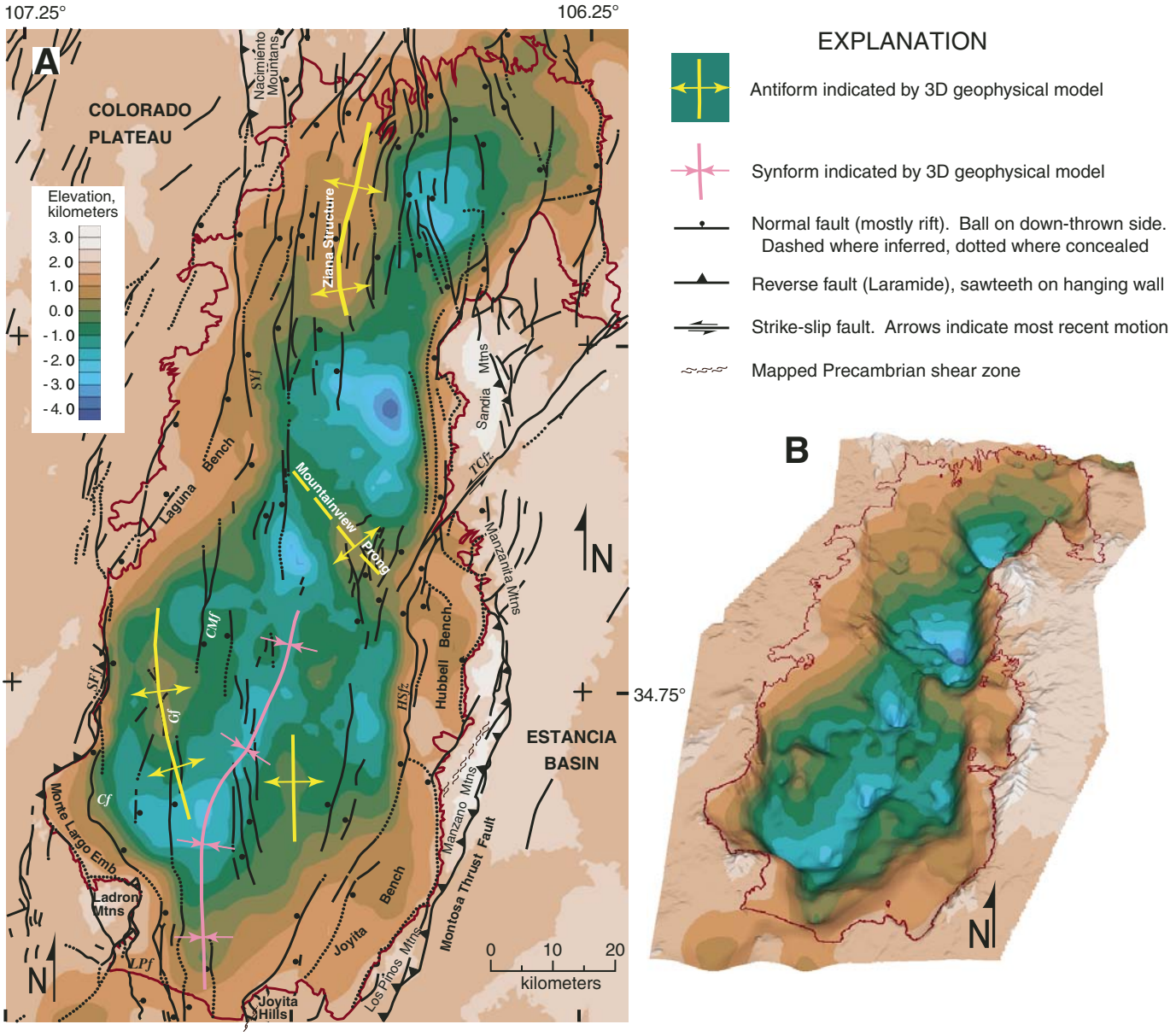

Figure 6. Structural elevation on the base of the Santa Fe Group derived from the final three-dimensional (3D) geophysical model merged with smoothed topography at the rift flanks. These views conceptually show the Albuquerque Basin as though the rift fill were removed. (A) Plan view of elevation above sea level with color interval of 0.5 km. The model contours have generally good correspondence to mapped faults from Figure 1. Cf—Coyote fault; CMf—Cat Mesa fault; Gf—Gabaldon fault; HSfz—Hubbell Spring fault zone; LPf—Loma Pelada fault; SFf—Santa Fe fault; SYf—San Ysidro fault; TCfz—Tijeras-Cañoncito fault zone. emb.—embayment. The basin boundary of Figure 1 (red-brown line) is overlain for reference. (B) Perspective view, using the same color scheme as the plan view. The relief is shown at 4:1 vertical exaggeration. The basin boundary of A is overlain for reference, with additional depiction of isolated outcrops of pre-rift rocks within the basin (see Fig. 1).

rhombohedral basin that ranges from 20 to 35 km wide (inset on Fig. 5; Fig. 6). However, the model is poorly constrained in this area because subsurface data are lacking (Fig. 3). The deepest part of the depression (3–4 km deep) is centered under Santa Ana Mesa, which is covered by Pliocene basaltic lavas (QTv on Fig. 1). The steep gradients of the model surrounding the broader expression of the Santo Domingo subbasin correspond in large part to major mapped faults, although the northwest boundary trends obliquely to several north-south mapped faults (Fig. 6), as noted earlier by Minor et al. (2006) and Grauch et al. (2006). These workers suggest that the northwestern side of the subbasin may have originated as an earlier northeast-striking fault system associated with basin-margin fault activity that was once focused on the western side of the Santo Domingo subbasin (Smith et al., 2001).

The 3D geophysical model shows the Calabacillas subbasin generally as an asymmetric half graben that deepens to a maximum of 4–5 km from southwest to northeast and west to east. The subbasin has two elongated north-south extensions on the southeast and northwest sides. The northwest extension lies on the west side of the Ziana structure (Fig. 6; Ziana anticline of Black and Hiss, 1974; Ziana anticlinal accommodation zone of Stewart et al., 1998), which is a south-plunging anticlinal horst. The southeast extension lies on the northeast side of the Mountainview prong. The northwest-trending Mountainview prong forms the southwest boundary of the Calabacillas subbasin. The eastern edge of the Laguna structural bench forms the western boundary of the subbasin, in the vicinity of the east-down San Ysidro fault (SYf on Fig. 6). A narrow zone of concealed, down-to-the-west, north-south–striking normal faults coincides with the modeled eastern border, ~1–7 km west of the Sandia Mountains rift-flank uplift (generalized on Fig. 1; Connell, 2008b).

Outlined by gentle to steep slopes that roughly form a hexagonal shape (inset on Fig. 5), the Belen subbasin is a composite of elongated structural ridges and troughs of varying symmetry. The northwest and southeast sides of the subbasin are bounded by the Laguna and Joyita benches, respectively; the west and east sides by the Santa Fe fault and the Hubbell bench, respectively; and the northeast and southwest sides by the Mountainview prong and the Coyote fault, respectively (Fig. 6). The northern half of the subbasin is dominated by mostly north-south–elongated structural ridges and troughs. Maximum thicknesses of the Santa Fe Group in the troughs range from ~3.0 to 3.5 km, with a deep depression (~5 km) southwest of the Mountainview prong. In the southwest, the Monte Largo embayment has a crescent shape, with a gentle slope on the outer edges that descends abruptly along a steep, curvilinear gradient that parallels the Coyote fault (CF on Fig. 6). This depiction is similar to previous concepts from Kelley (1977), who suggested the presence of a structural bench on the west that is bounded by the Coyote fault. A series of poorly defined, northeast-trending steps cuts diagonally across the southeastern Albuquerque Basin, and forms the northwest side of the Joyita bench. A large part of the Joyita bench is occupied by a graben that is most noticeable in the model in the northeastern part of the bench.

As earlier noted by Kelley (1977), the southern Albuquerque Basin narrows to a constriction formed by the convergence of the eastern and western structural borders. The southwestern border includes the Coyote fault combined with the south-trending Loma Pelada fault along the eastern side of the Ladron Mountains (LPf on Fig. 1). The eastern border is represented by the northeast-striking boundary of the Joyita structural bench.

Basin Tilts

Determining the dip of strata above the basin floor is critical for understanding the tilt of subbasin half grabens and strain-accommodation zones. The 3D geophysical model only provides dips of the basin floor as determined from the variations in rift-fill thickness, so we compare seismic information and geologic mapping to establish stratal tilts. We focus on tilts of the Miocene strata, because this age represents the bulk of the rift fill represented by the 3D geophysical model and predates the development of a widespread unconformity between Miocene and Plio-Pleistocene strata (Connell et al., this volume).

As demonstrated for seismic lines 81, 48, and 53 in the following sections, the interpreted base of Santa Fe Group from the 3D geophysical model typically shows excellent conformity to the tilts of migrated and depth-corrected seismic reflections. In addition, exposed Miocene Santa Fe Group strata have measured attitudes that correspond well to the form of the modeled structural elevation grid along the west-central Belen subbasin and flanking the eastern and western sides of the Santo Domingo subbasin (Appendix G [available on CD-ROM accompanying this volume and in the GSA Data Repository (see footnote 1)]). This correspondence between measured and modeled dips, along with the correspondence of northeastern tilts of the model in the Calabacillas subbasin with stratigraphic correlations of well data (Connell et al., 1998), allow us to use the thickness model to infer overall tilts of the Miocene Albuquerque Basin, with the caveat that basin-floor tilts may also be accommodated by normal faults that step toward the basin margin.

We do not have information on stratal tilts of the older Santa Fe Group in the Santo Domingo subbasin and the Monte Largo embayment in the southwestern corner of the Belen subbasin. Because the Santo Domingo subbasin has tilted in opposite directions at different periods during late Miocene to Pleistocene time (Smith et al., 2001; Minor et al., this volume), we infer that the somewhat symmetric basin geometry represents a composite of the alternating tilts through time. In the Monte Largo embayment, we infer that strata are tilted southwest against the Coyote fault because (1) westward tilts are implied by the Russell-Snelson model (Fig. 2B), (2) the area appears connected to the small west-tilted half graben observed near the west side of profile C–C′ (Fig. 6), and (3) the thickness model defines a wedge-like volume, with the curvilinear Coyote fault bounding the thickest part of the wedge on the southwest.

Miocene basin tilts are predominantly easterly (east to northeast) throughout the Albuquerque Basin, except for westerly (west to southwest) dips in the southwestern portion and other variations in a few local areas. Examination of the thickness model suggests that easterly tilted basin floor generally dips ~5°–10° across broad areas (as much as ~25 km width), whereas westerly tilted basin floor dips ~9°–15° across narrower areas (as much as ~15 km width). Within the Belen subbasin, the transition from predominantly easterly tilts in the north to westerly tilts in the southwestern portion is not simple or clearly defined.

Regional Implications

The increasing size and complexity of subbasins from north to south in the Albuquerque Basin may reflect the transitional character of this basin within the Rio Grande rift, as noted by

previous workers (e.g., Cordell, 1978). The basin lies between physiographically and structurally well-defined rift basins to the north and segmented, linked rift basins within a broader region of crustal extension associated with the Basin and Range province to the south. The Santo Domingo subbasin may represent a broad zone of strain accommodation between the west-tilted Española Basin and the east-tilted Calabacillas subbasin (Smith et al., 2001; Minor et al., this volume). In turn, the Belen subbasin may reflect a broad zone of strain accommodation between the east-tilted Calabacillas subbasin and the west-tilted Socorro Basin on the south. The Belen subbasin contains multiple, elongated structural ridges and troughs of varying symmetry that give the basin a highly segmented geometry, similar to the patterns within the Socorro Basin and rift basins farther south.

MODEL VALIDATION

Evaluation of the model was a critical part of model development. We constructed 2D geophysical models and geologic cross sections, and examined seismic sections before adding information from them as constraints in subsequent inversion runs to arrive at a final, fully constrained 3D geophysical model. During this process, conflicts with previous models and interpretations were reconciled. In this section, we present several of these evaluations that are key to validating the model as a whole. Additional discussion of these and other evaluations are presented in Appendix G.

Eastern Rift Borders and the Mountainview Prong

Examination of migrated depth sections for the reprocessed seismic data from north-south lines 59 and 85 (Fig. 3; Appendix F) verifies results of the initial 3D gravity model for the eastern side of the Albuquerque Basin (Fig. 7). These semi-parallel lines from the Shell data set, which were not included in the Russell-Snelson model, cross the gravity-defined Mountainview prong and reach into both the Calabacillas and Belen subbasins. Reflections from the migrated depth section for line 85 were tied to lithologic picks in the Transocean #1 Isleta well (Fig. 3). These reflections and two others recognized within the Tertiary section can be followed to the north and south in this and the depth migrated section for line 59, showing an antiformal structural culmination that corresponds with the observed gravity high that defines the Mountainview prong (Fig. 7).

Peaks of the gravity high associated with the Mountainview prong generally coincide with the crest of the structural culmination depicted by both interpreted seismic sections (asterisks on Fig. 7), supporting a northwest trend for the Mountainview prong. Despite a north-south gradient that marks an abrupt increase in thickness 5 km west of the crossing of lines 85 and 65 (Fig. 5B), the gravity anomaly suggests the Mountainview prong extends (at lower structural levels) 15 km farther northwest of the north-south gravity gradient. No other seismic lines cross this gravity feature, except at the very northwest end in the area east and south of the Carpenter Atrisco #1 and Utex 1-1J1E Westland Development wells, respectively (Fig. 3).

Thus, the existing seismic data support the gravity-defined Mountainview prong and the deep parts of the Calabacillas and Belen subbasins east of the Rio Grande. The seismic sections also provide additional constraints that we applied to the inversion to arrive at the final 3D geophysical model (Fig. 5B). Points were picked along the seismic horizon interpreted as the base of the Santa Fe Group for both lines 85 and 59. Points were also picked at the farthest northwestern extent of the gravity expression of the Mountainview prong by estimating the thickness from the Russell-Snelson model (May and Russell, 1994) in an area of good seismic coverage (cf. Figs. 2B and 5B). In comparison to the initial 3D gravity model, these constraints resulted in refinements in the final 3D geophysical model to the width of the Mountainview prong and moderated the depth of a local excursion within the Calabacillas subbasin that the 3D inversion created just to the north of the Mountainview prong (cf. Figs. 5A and 5B).

Support for the presence of thick rift fill next to the Hubbell bench is underscored by a more extensive, north-south 2D integrated geophysical model along profile A–A′ that crosses the Belen subbasin (Fig. 8). The 2D model incorporates interpretations from seismic line 59 and integrates gravity and aeromagnetic data. The model is consistent with interpretations from crossing seismic lines, profile C–C′, Grober-Fuqua #1 well (Table 1), a magnetotelluric sounding (MT10, Fig. 3), and magnetic depth estimates. The top of the resistor indicated for MT10 may represent the shallowest occurrence of resistive rocks, such as the basal marine limestones of the upper Paleozoic succession (Rodriguez and Sawyer, this volume). However, the depth is only constrained to within 1 km (B. Rodriguez, 2009, personal commun.). Geologic units in the 2D model are assigned the appropriate density-depth functions (Fig. 4; Appendix D). Pre-rift units are grouped (shown as one color) below a depth of 3.25 km because they cannot be distinguished from each other solely on the basis of density contrast. Unlike the pre-rift units, the Santa Fe Group has fairly large, negative density contrasts with the densities of all the older units over the entire depth range of the model. In fact, the negative density contrasts are the primary cause of the shape of the gravity curve along this line, as demonstrated by the good fit of the curve computed only from the model bodies representing the Santa Fe Group (thick green line plotted with the gravity curve on Fig. 8).

The fit to the aeromagnetic data in the model of profile A–A′ is intentionally left fairly loose. The gross features of the aeromagnetic curve are caused mainly by magnetic rocks that make up the Proterozoic basement or possibly by buried volcanic rocks resting on the Joyita bench at the south end of the profile, which was not modeled. The buried volcanic rocks are inferred from patterns on the aeromagnetic map compared to exposures of Oligocene volcanic rocks ~6 km to the southwest near Black Butte, in the southeastern part of the Albuquerque Basin (BB on Fig. 1). The modeled Proterozoic basement is primarily constructed by variations in magnetic properties and relief on the top of the

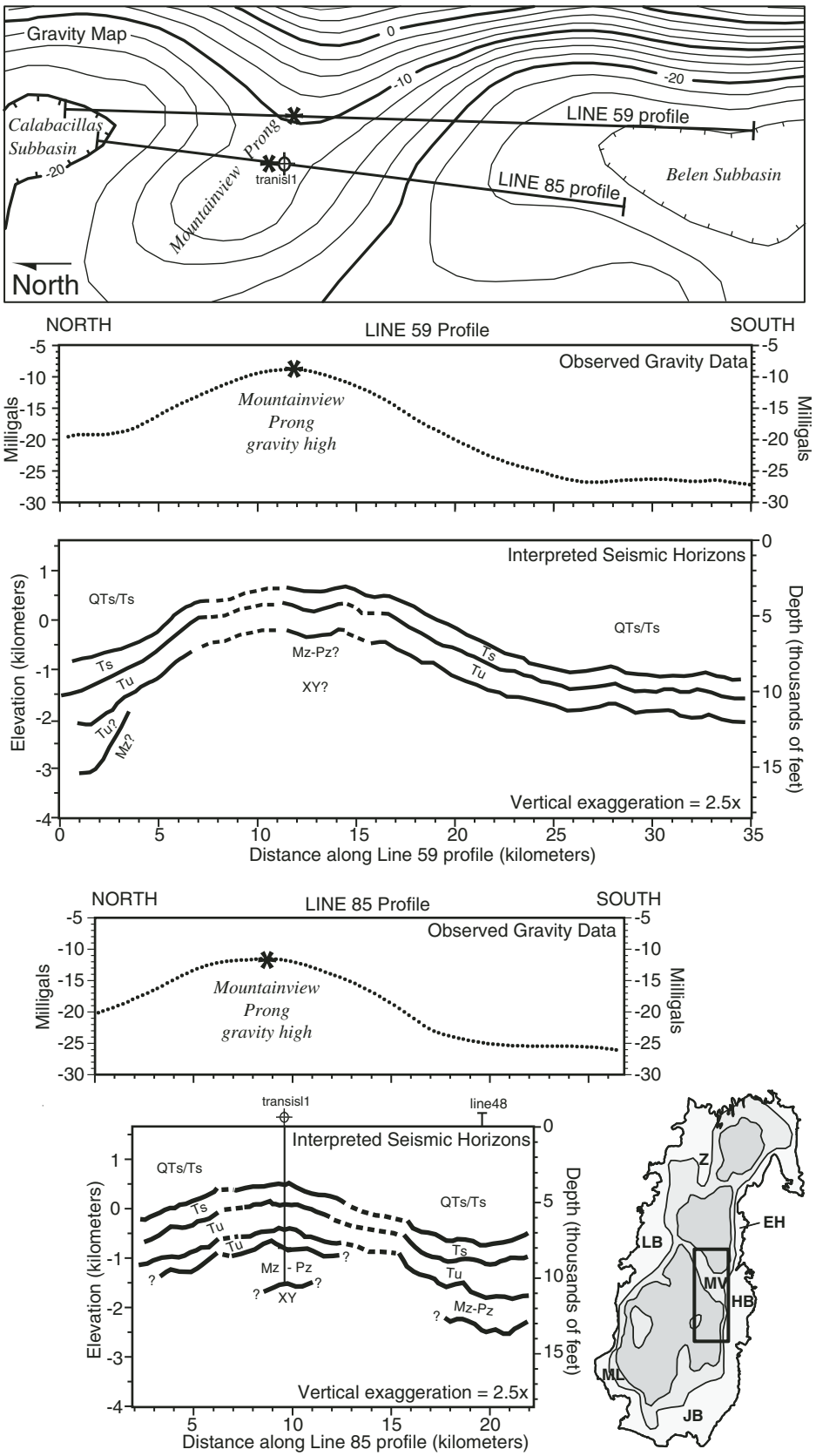

Figure 7. Antiform interpreted from seismic-reflection data corresponding to the northwest-trending gravity high associated with the Mountainview prong. Seismic interpretations are from reprocessed, migrated depth sections for lines 59 and 85 located on Figure 3. Horizons interpreted from the migrated depth sections (Appendix F [available on CD-ROM accompanying this volume and in the GSA Data Repository (see footnote 1)]) are tied to picks in the Transocean #1 Isleta (transisl1) well (Black, 1982; Lozinsky, 1994). Geologic unit codes are from Figure 1 except where undifferentiated: QTs/Ts indicates undifferentiated Santa Fe Group; Tu indicates undifferentiated Oligocene and Paleocene units (Tis and Tel). Horizons are interpreted *within* some of these units on the basis of strong seismic reflections. Gravity data are shown in map view (north is to the left) and in profile for each interpreted seismic section. Map contour interval is 2.5 mgals. For reference, asterisks at the peaks of the gravity high along the profiles are noted on both the profiles and the map. The map area is indicated on the inset subbasin index map (from Fig. 5).

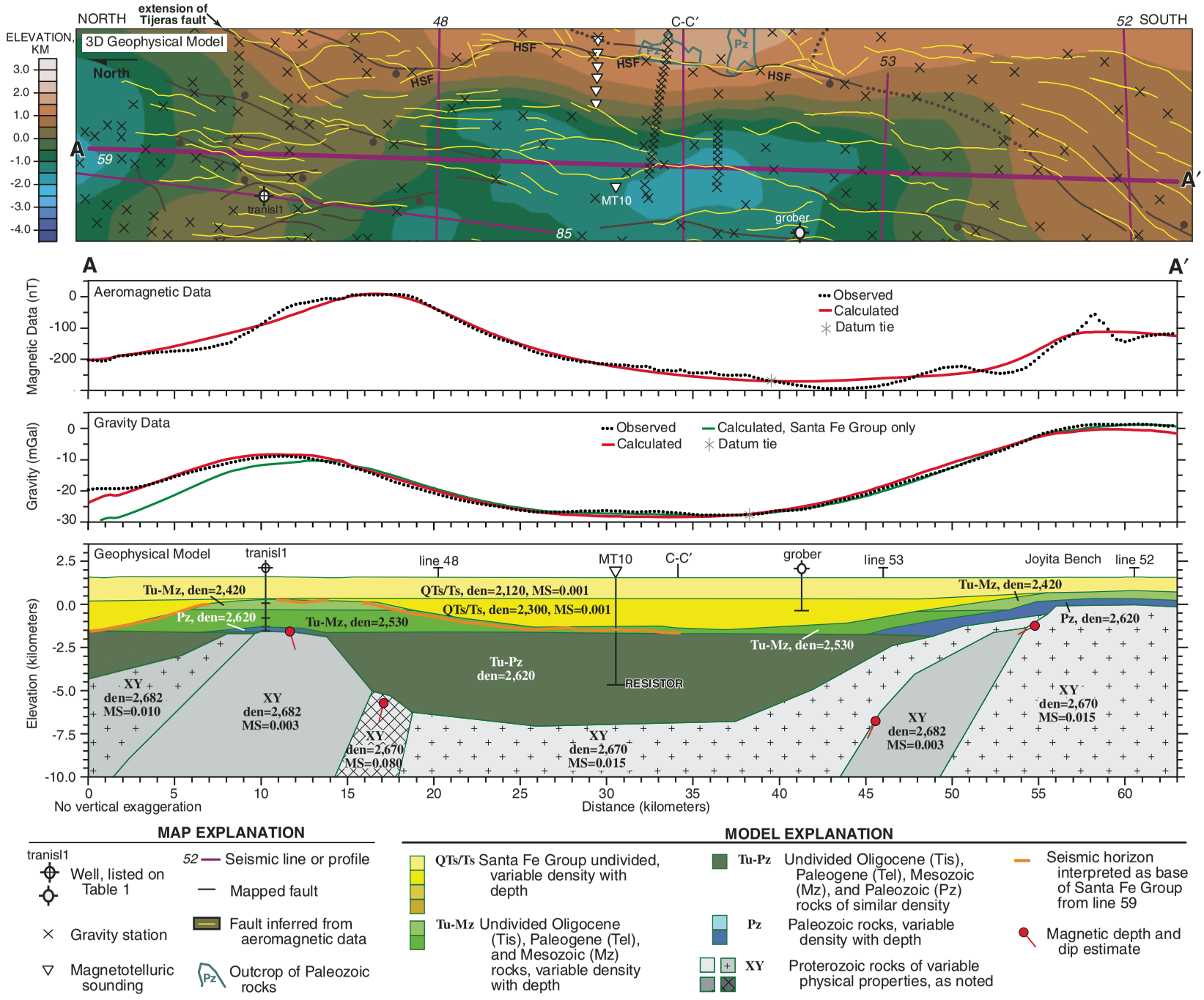

basement, with some control provided by gravity data. Because the basement bodies are poorly constrained, we attempted to keep the magnetic-property variations to a minimum and used magnetic depth and dip estimates to loosely guide the deeper part of the model (solid red circles with tails on Fig. 8).

The 2D model shows that all data integrated together support as much as 3 km of Santa Fe Group within the Calabacillas and Belen subbasins to the north and south of the Mountainview prong along the eastern side of the Albuquerque Basin. The profile is mostly parallel to normal faults in the area (map view on Fig. 8), so it represents only a general longitudinal view of these subbasins. The Joyita structural bench occurs on the far south side of the model, showing a northeasterly strike in plan view and rising to depths of ~1 km on the south (Fig. 8).

Calabacillas Subbasin

The 3D gravity model shows the Calabacillas subbasin as an asymmetric half graben that deepens to a maximum of 4–5 km from southwest to northeast and west to east. This basin geometry is supported by an integrated geophysical model and geologic cross section across the middle of the subbasin along profile B–B′ (Fig. 9). The geologic cross section is modified slightly from Connell (2008b), who used well data and detailed mapping to extrapolate geologic relations into the deeper parts of the basin. The gravity and magnetic model for profile B–B′ translates the units of the geologic cross section into polygonal bodies with density and magnetic properties. Starting with an initial geologic cross section constructed independently, we used fits to the computed fields of the model to refine the configuration of the deeper parts of the cross section, which are poorly constrained by geology. The 2D geophysical model provides the most information on the configuration of the structural blocks that make up the eastern boundary fault area, driven mainly by the large density contrast between the Santa Fe Group and the denser, older rocks at the boundary (Fig. 9). A thin pre-rift sedimentary section on top of the easternmost structural blocks gave the best fits in the gravity and magnetic model. The high density assigned to the Proterozoic basement within part of the uplifted eastern basement block is required to fit the 2D model to known geologic constraints, given the good constraints in this area on densities of the younger rock units and depths to the relatively shallow basement. A high density for the basement in this area of the 2D model is also supported by the 3D gravity inversion; a large high in the regional field resulting from the inversion trends north-northwest in the vicinity of the western front of the Sandia Mountains (Appendix E).

A curve representing the base of the Santa Fe Group extracted from the initial 3D gravity model is overlain on the 2D model of profile B–B′ (red dotted line on Fig. 9). The comparison underscores that both 2D and 3D approaches to modeling and integrating the data sets arrived at similar results. The mismatches between the 3D gravity model and the integrated 2D geophysical model and geologic cross section also demonstrate some of the geophysical model limitations: the 3D gravity model smooths large structural discontinuities (i.e., faults) on the west and east sides, and mismatches in the deepest parts of both models may arise from differences in 2D versus 3D representations of the structure or density. Considering these limitations, the fit of the initial 3D gravity model and the geologic cross section is fairly good.

Northern Belen Subbasin

Isopach maps for both initial and final 3D models for the central part of the Albuquerque Basin show depocenters on the southwest and northeast sides of the Mountainview prong (Fig. 5). Previous workers who modeled gravity profiles across this part of the basin also recognized two depocenters and an intervening structural high (Birch, 1982, his profile 5; Peterson and Roy, 2005, their profile C). The 3D model shows that the northeastern depocenter is a southern extension of the Calabacillas subbasin and the southwestern depocenter, the Mountainview half graben, is a structural element of the northern Belen subbasin.

The presence of the Mountainview half graben is documented by deep wells and by seismic-reflection and gravity data, although its exact boundaries are ambiguous (Appendix G). Russell and Snelson (1994a) and May and Russell (1994) used east-west–oriented seismic lines 65 and 72 (Figs. 3 and 5) to show it as an east-tilted half graben bounded on the east by a listric normal fault—their Rio Grande fault. They considered the Mountainview half graben to represent the east-tilted northern

Figure 8. North-south two-dimensional (2D) geophysical model along profile A–A′ (Fig. 3). Top section (north is to the left) shows structural elevations of the base of Santa Fe Group derived from the final 3D geophysical model. Mapped faults are from Figure 1; aeromagnetically interpreted faults are from Grauch and Hudson (2007). Lower section shows the model, locations of independent constraints from Figure 3, and calculated and observed data curves. Interpretation of magnetotelluric sounding MT10 is from Rodriguez and Sawyer (this volume). Magnetic data are only loosely fit to constrain major features, which are dominated by basement sources. Model bodies vary in color and pattern according to bulk density (den) in kg/m^3 and magnetic susceptibility (MS) in Système International (SI), respectively. Densities for sedimentary units are assigned according to derived density-depth functions (Table 2; Fig. 4). Density variations with depth are depicted by subhorizontal boundaries that are not intended to represent stratigraphic contacts. Physical properties for Proterozoic rocks come primarily from the model fit (see text). Magnetic susceptibilities may include a component of remanent magnetization. Magnetic susceptibilities assigned to the Santa Fe Group represent a typical order of magnitude from measured samples (Hudson et al., 2008). Magnetic depth and dip estimates used the multisource Werner method (Hansen and Simmonds, 1993), with a 2.1 km window size and 8–16 solutions per cluster (Appendix C [available on CD-ROM accompanying this volume and in the GSA Data Repository (see footnote 1)]). Model bodies representing Santa Fe Group are truncated ~7 km north of the profile to account for 3D effects caused by the termination of the basin near the Hubbell Spring fault (HSF).

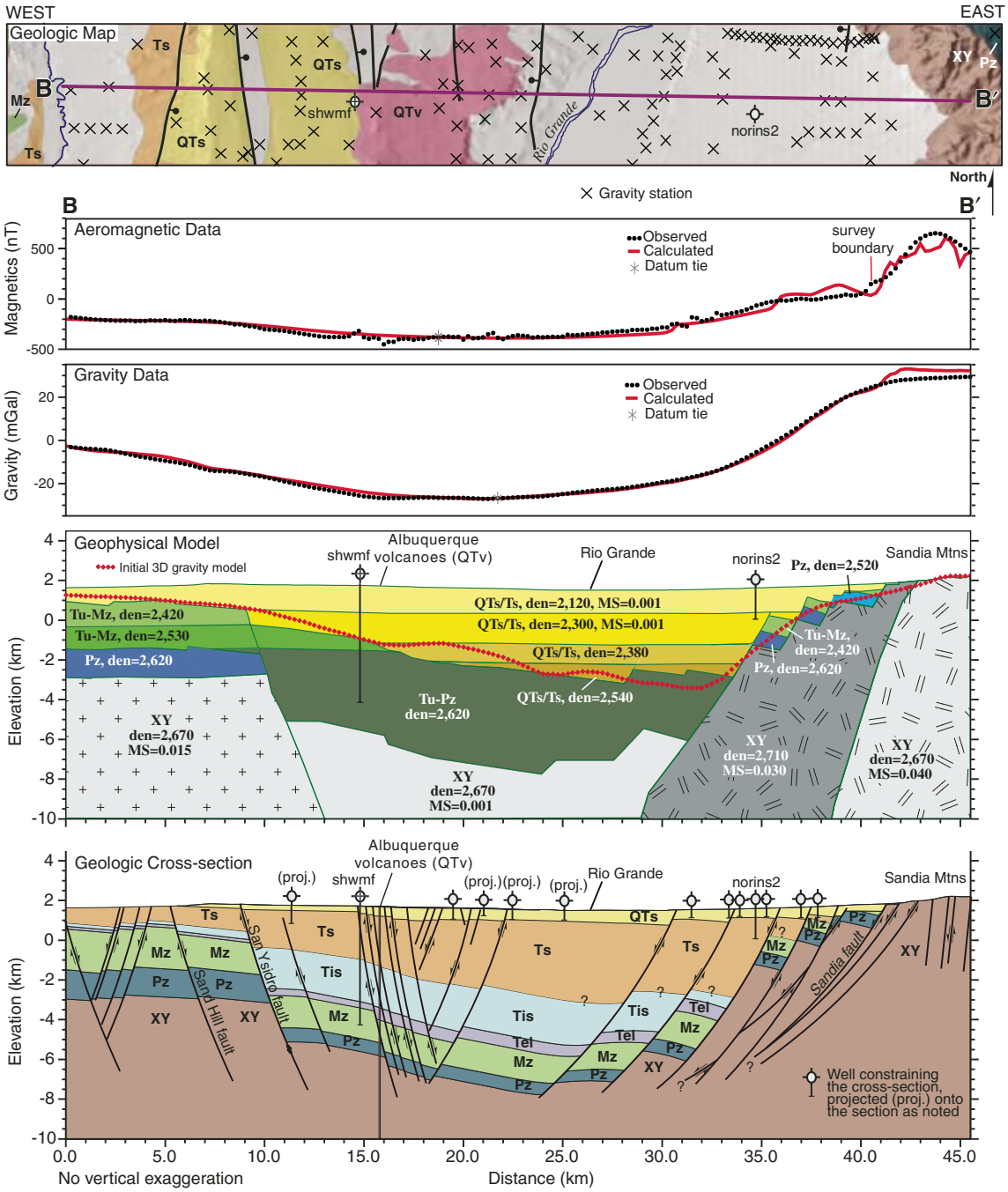

Figure 9. West-east two-dimensional (2D) geophysical model and geologic cross section along profile B–B′ in the northern Albuquerque Basin (Fig. 3). Top section shows locations of gravity stations on a geologic strip map from Figure 1. Geologic codes on the map and cross section are described in Figure 1. Codes for the geophysical model bodies and the assignments of physical properties are explained in Figure 8. Well codes are from Table 1.

Albuquerque Basin and the Rio Grande fault to represent the eastern border of the deep rift (Fig. 2B). We suggest instead that the Rio Grande fault in this location is actually the western boundary of the Mountainview prong, and that the eastern boundary of the Albuquerque Basin (Calabacillas subbasin) is ~15 km farther east (Fig. 5).

Central Belen Subbasin

In the central part of the Belen subbasin, the initial 3D gravity model depicts several northerly elongated highs and lows bordered by steep gradients (2–3 km relief) on the east and west sides of the subbasin (Fig. 5). The depression adjacent to the Hubbell bench

already has been examined longitudinally (north-south) along profile A–A′ (Fig. 8). We construct a geologic cross section and 2D geophysical model along profile C–C′ to evaluate the model configuration in the east-west direction. Because of irregular seismic coverage, we considered several seismic lines on the west and east sides of the Belen subbasin before constructing the cross section for C–C′ in an intervening location with suitable gravity station coverage. Concepts from line 81 guided the construction of the western portion of profile C–C′, whereas concepts from lines 53 and 48 guided the central and eastern portions (Fig. 5B).

Shell seismic line 81 closely follows the western portion of profile C–C′. A time section for this line was available to us only as a scanned image from Russell and Snelson (1994a) and as a line drawing of reflections from May and Russell (1994). Figure 10 shows the line drawing overlain by the corresponding curve from the initial 3D gravity model after depth-time conversion according to Table 2. The model curve represents the base of the Santa Fe Group resulting from the gravity inversion, with a thickness constraint of 1494 m (~1.4 s TWTT) under the Humble Shell Santa Fe #1 well (humsf1 on Table 1; Fig. 3). The model curve closely follows the general form of the seismic reflections to the east and west of the well. The correspondence between the reflections and the model curve supports the interpreted base of the Santa Fe Group from both seismic and gravity data. The configuration of the interpreted base in relation to the seismic section implies that (1) Santa Fe Group thickens and dips both east and west, (2) the dip of the basin floor reflects the sense of stratal tilt, and (3) seismic reflections below the model curve on line 81 represent pre–Santa Fe Group rocks.

Although reflection multiples may be present in the apparently unmigrated seismic section for line 81, the shallow dips of the reflections and consistencies after depth-time conversion suggest that Santa Fe Group strata have decreasing dip upsection on both the east and west portions of the line (Fig. 10). These relations imply that half-graben–style tilting occurred in both directions (although not necessarily contemporaneously), with corresponding master faults both to the east and west. The low-angle fault on the west side of line 81 ("fault" on Fig. 10) appears to be the boundary fault for the western, smaller half graben. The shallow dip of the fault shown on the seismic section (~30°E after simple time-depth conversion) is close to measured fault dip farther west, and is supported by gravity modeling (presented below; Birch, 1982, his profile 10). A faulted antiform is the focal point for the hinge zones of the two half grabens and generally corresponds to a buried, structural high that involves Precambrian basement. The boundary fault for the eastern half graben must be east of the seismic line.

Data obtained and reprocessed by the USGS for the eastern parts of seismic lines 53 and 48 cover the southeastern and northeastern sides, respectively, of the Belen subbasin (Fig. 5B). Interpretations of migrated depth sections for these data (Fig. 11) serve as analogs for constructing the central and eastern portions of the model for profile C–C′, with the caveat that where they cross profile A–A′, they are located in shallower parts of the basin than is profile C–C′ (inset on Fig. 11). The seismic section for line 53 shows fairly good-quality reflections, but little independent information is available to constrain the interpretation. Well data and geologic information are better for line 48 than for line 53, but the quality of the seismic data is worse. In areas of poor data quality on line 48, we relied heavily on the interpretations developed for crossing seismic lines 85 and 59 (Fig. 7 and Appendix F). Despite the limitations to seismic interpretation of these sections, the base of the Santa Fe Group could be generally interpreted. Moreover, patterns of reflections reveal conceptual information about the rift basin and its relation to the underlying structure. Uninterpreted depth sections and details on the interpretations are included in Appendix F.

Similar patterns of reflections are apparent between 12 and 19 km distance on line 48 and 5–12 km distance on line 53. The patterns suggest that the lower part of the Santa Fe Group section and part of the underlying, older section form a faulted synform overlying unconformable, west-dipping basal high-amplitude

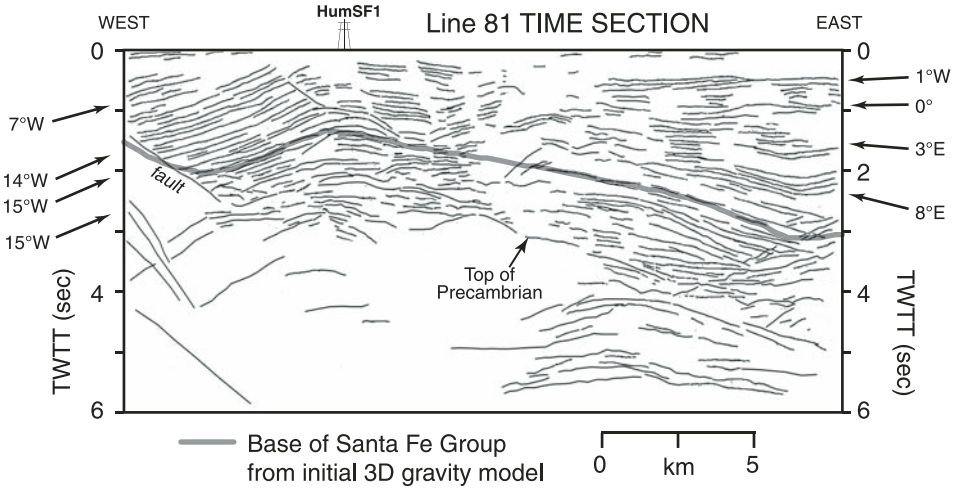

Figure 10. Interpretive line drawing of Shell line 81 time section modified from May and Russell (1994), located at the western side of the central Belen subbasin (Fig. 3). Time-converted curve (following Table 2) was extracted from the initial three-dimensional (3D) gravity model (Fig. 5A) and superimposed (semi-transparent black line) on the seismic section. Arrows indicate angled reflections in the Santa Fe Group section, with representative dips computed after conversion to depth. Dips increase with depth on both sides of line 81, suggesting that the basin has tilted both to the east and west. An antiform under the Humble Shell Santa Fe #1 well (HumSF1; Table 1) appears to accommodate opposing stratal tilts. TWTT—two-way travel time.

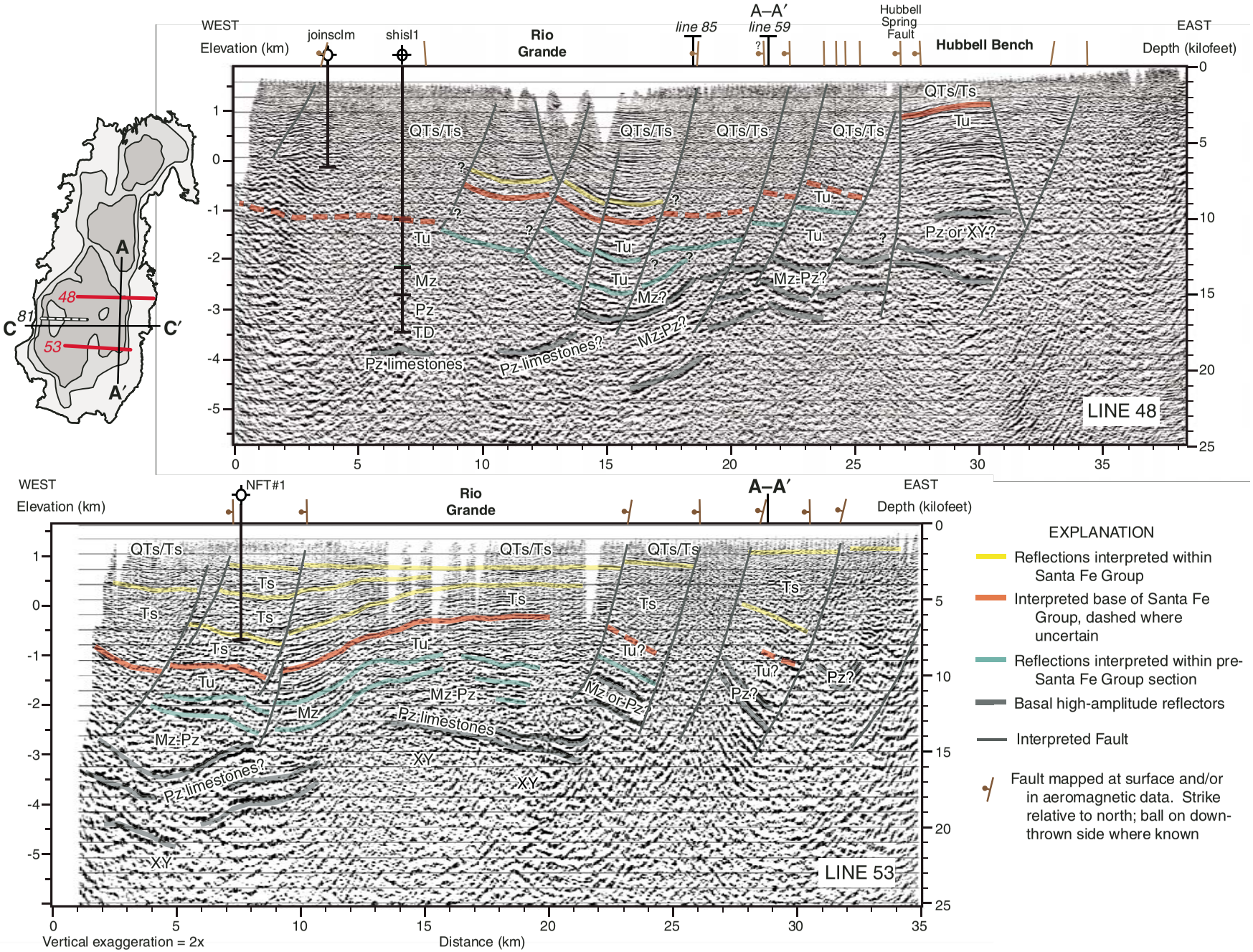

reflections, interpreted as the lower part of the Phanerozoic section (Appendix F). The synform has varying asymmetry from north to south, with steeper western limb on line 48 on the north and a steeper eastern limb on line 53 on the south. On line 53, west-dipping Santa Fe Group reflections (yellow lines on Fig. 11) show decreasing dip up-section between 9 and 15 km distances, whereas underlying layers have more consistent thickness, suggesting Miocene deposition. Moreover, reflections between 0 and 4 s on the eastern 8 km of the time section for line 81 (Fig. 10) show similar patterns to those on the depth section for line 53 between distances 1 and 9 km down to elevations of −5 km (Fig. 11). The similarity suggests that the eastern half graben on line 81 is analogous to the eastern limb of the depocenter on line 53. If so, the eastern half graben on line 81 may be bounded on the east by a separate depocenter rather than a basin-bounding fault. On the other hand, a better-defined boundary fault may be represented by the inferred, west-down fault offsetting the base of Santa Fe Group on line 48 between the Rio Grande and Shell 1 Isleta well (shisl1).

East of the synform, patterns of reflections are somewhat dissimilar between the two seismic lines (Fig. 11) except that both show fault blocks that step down to the west from the Hubbell bench. We interpret parallel, east-dipping basal high-amplitude reflections on line 53 between distances 14 and 22 km as Paleozoic limestones capping an east-dipping, basement-cored horst of probable Ancestral Rocky Mountain (late Paleozoic) origin (Appendix F). Such a horst was postulated in this area by Baars (1982) and is analogous to a west-dipping horst in the Joyita Hills at the southern end of the basin (Beck and Chapin, 1994) that is also captured in seismic sections from the COCORP lines and Shell seismic line 52 (Fig. 3; de Voogd et al., 1988; Russell and Snelson, 1994a). On line 48, the discontinuous eastward rise of west-dipping basal high-amplitude reflections and inferred variations in thickness of pre-rift strata suggest tectonic disruption by pre-rift tectonic activity. The pattern is reminiscent of Laramide-style reverse faulting observed in the mountains flanking both sides of the southern part of the Albuquerque Basin (Cabezas, 1991). In these areas, a set of east-verging low- to high-angle reverse faults cut west-dipping Paleozoic strata, with tight, overturned folds ahead of the thrust front.

Figure 11. Interpreted migrated-depth sections for seismic lines 48 and 53. Inset (from Fig. 5) shows line locations in relation to line 81 and profiles A–A′ and C–C′. The two depth sections shown are aligned at the crossings of profile A–A′. A synform between distances 7–12 km on line 53 is also evident between distances 13–18 km on line 48. Geologic codes are the same as in Figure 1 except: QTs/Ts—all Santa Fe Group; Tu—Tis and Tel (undifferentiated). The lower part of the Santa Fe Group section is inferred as Ts, but no interpretation of the contact between QTs and Ts is intended here. Seismic data are owned or controlled by Seismic Exchange, Inc.; interpretation is that of the U.S. Geological Survey. Interpretations are described in Appendix F (available on CD-ROM accompanying this volume and in the GSA Data Repository [see footnote 1]).

Using the concepts from the three seismic lines (Figs. 10 and 11) to constrain rift structure and postulated pre-rift structure from lines 48 and 53, we iteratively constructed a geologic cross section and 2D geophysical model along profile C–C′ (Fig. 12). The magnetic data were fit only loosely to help constrain steep basin boundaries. As with profile A–A′, most of the magnetic anomalies appear to be caused by intra-basement sources that can be fit by a large number of configurations and thus do not shed light on the basin geometry. As with the previous 2D models, the small density contrasts between the pre–Santa Fe Group units, especially at depth, prevent their robust distinction from the gravity modeling alone.

The 2D geophysical model for profile C–C′ places constraints on the configuration of the rift fill and matches the geologic cross section. Thickness of rift fill varies from ~1.5 km to 3.0 km across the model, with alternating highs and lows, as indicated by the initial 3D gravity model in plan view (Fig. 5A). The highs and lows depict a narrow west-tilted half graben on the west side and gently undulating to east-tilted structural blocks across most of the Belen subbasin. The synform occurs near the middle of the subbasin, with its axis at ~32 km distance on profile C–C′. A well-defined east-tilted half graben on the east side of the basin is bounded by a steep fault ~1 km west of the Hubbell Spring fault mapped at the surface. The shallow dip of the rift-bounding fault on the west side of profile C–C′ is supported by gravity, magnetic, and seismic data (Figs. 10 and 12). The thickened pre-rift section in the deep basin adjacent to the Hubbell Spring fault zone is suggested by reconstructions of the geologic cross section (Appendix G) and the crossing geophysical model along profile A–A′ (Fig. 8). In general, the thickness of rift fill across this model shows a basin with less asymmetry and generally more-moderate values than the 2D model across the Calabacillas subbasin (Fig. 9).

The faulted synform recognized in lines 48 and 53 and at the east edge of line 81 is recognizable, but incoherent in the initial 3D gravity model (Fig. 5A). After application of all thickness constraints (from line 53 and the profile C–C′ model in particular), the synform is more clearly defined in the final 3D geophysical model (Fig. 5B), where it trends north-northeast across much of the Belen subbasin.

Geologic interpretation of line 81 seismic section (Fig. 10) is at the crux of the major differences between the Russell-Snelson model and our 3D geophysical model in the Belen subbasin. Russell and Snelson (1994a) interpreted the section for line 81 as an east-dipping, low-angle detachment fault with blocks of west-tilted pre-rift strata rotated into the fault (Fig. 13). Even though May and Russell (1994) suggested that the west tilt of the blocks compared to the east tilt of seismic reflections is counterintuitive, the detachment fault interpretation, shown without depicting the dips of reflections, has been used by other workers to represent a west-tilted half graben for the southern half of the Albuquerque Basin (e.g., Lozinsky, 1994; Ingersoll, 2001, 2003; Johnson et al., 2001). We find the interpretation understandable, but in disagreement with the gravity data, and counterintuitive to

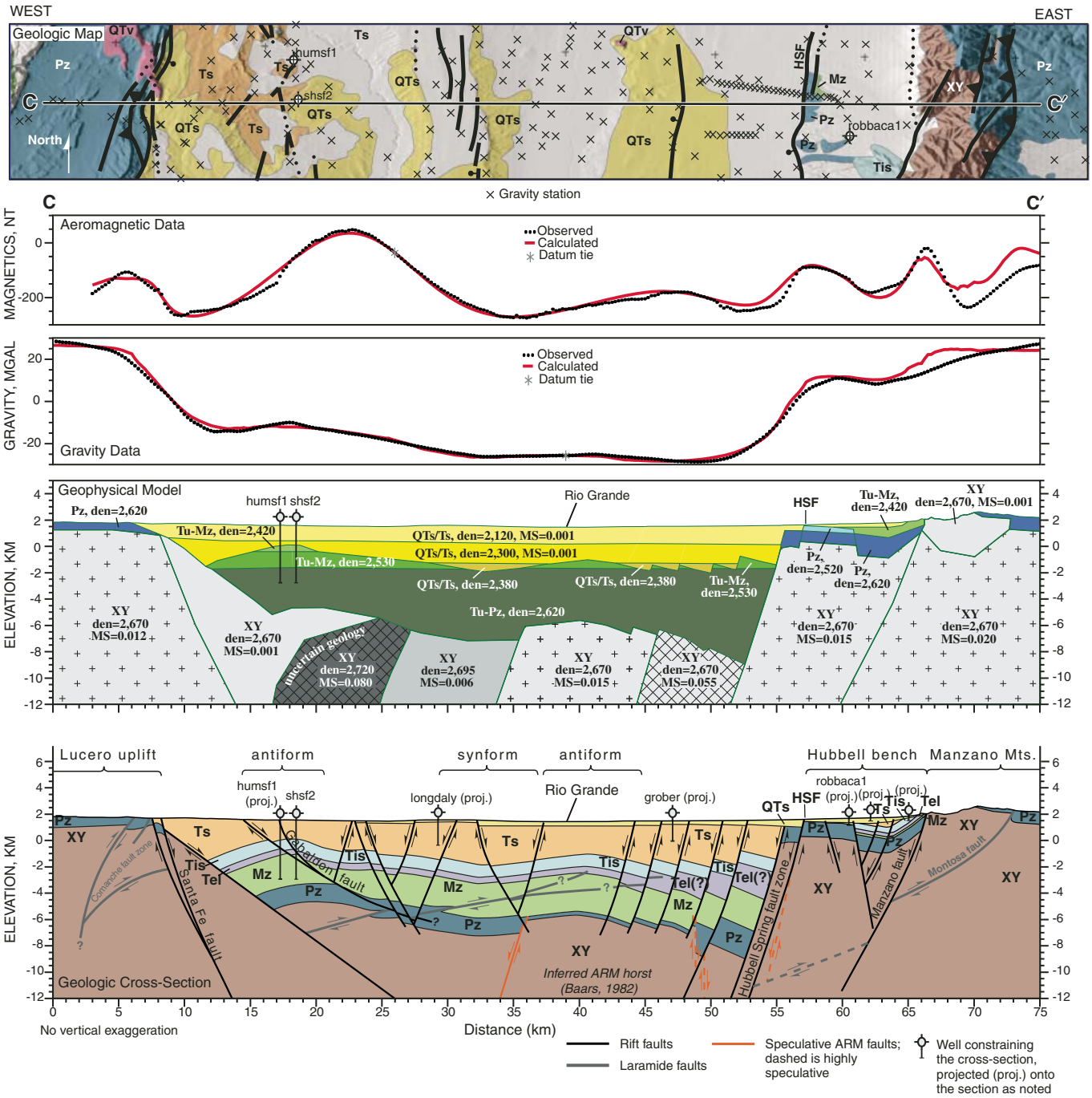

Figure 12. West-east two-dimensional (2D) geophysical model and geologic cross section along profile C–C′ in the southern Albuquerque Basin (Fig. 3). The cross section and model were constructed from synthesizing interpretations of seismic lines 81, 48, and 53 (Figs. 10 and 11). The overall thickness of the Santa Fe Group is fairly well constrained, but the configuration of older geologic units is open to different interpretations. Extremely magnetic intra-basement blocks (cross-hatching on the geophysical model) are required by the data at the depths indicated. However, their shapes are ambiguous and, as configured, are not intended to invoke any particular geologic interpretation. Ancestral Rocky Mountains (ARM) structures are discussed in text. Top section shows locations of gravity stations on a geologic strip map from Figure 1. Geologic codes on the map and cross section are described in Figure 1. Codes for the geophysical model bodies and the assignments of physical properties are as explained for Figure 8. Well codes are from Table 1. Additional discussion of the geologic cross section and its reconstruction are included in Appendix G (available on CD-ROM accompanying this volume and in the GSA Data Repository [see footnote 1]).

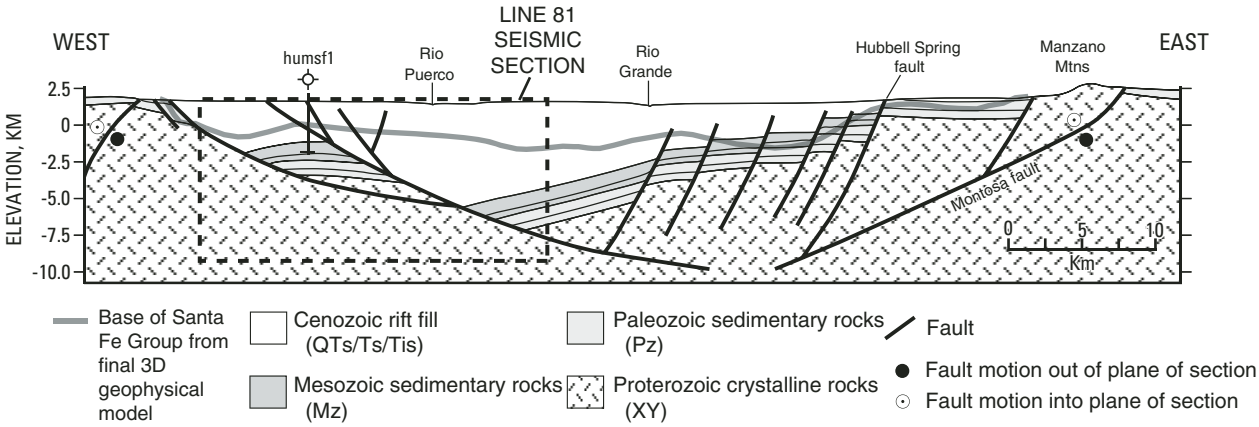

Figure 13. Geologic cross section across the southern Albuquerque Basin from Russell and Snelson (1994a) compared to the base of Santa Fe Group extracted from the final three-dimensional (3D) geophysical model (bold gray line). The cross section has been used to demonstrate a west-tilted half graben in the southern Albuquerque Basin and partially coincides with seismic line 81 (outlined by the dashed line). Based on the 3D geophysical model, stratal tilts are instead to the east, consistent with seismic reflections from line 81 east of the Humble Shell Santa Fe #1 well (humsf1) on Figure 10. Moreover, the large thickness of rift fill indicated by the cross section under Rio Puerco is not consistent with observed gravity data (Gillespie, 2002).

the seismic evidence. Gravity data instead support an eastward-deepening basin along this line, as shown by Birch (1982, his profile 10), Gillespie (2002), and our initial 3D gravity model (Fig. 10). Although our explanation of the structure of line 81 (as depicted in the geologic cross-section panel of Fig. 12) is only one of several geologic explanations possible, we argue that it is better substantiated than the Russell-Snelson model because it is supported by a broader array of independent data sets.

Southern Belen Subbasin

The southern part of the Albuquerque Basin has been the subject of intense study to understand the shallow structure of the Rio Grande rift and underlying crust since acquisition of COCORP seismic-reflection data in the 1970s (e.g., Brown et al., 1979, 1980; Jurdy and Brocher, 1980; Brocher, 1981; Cape et al., 1983; Wu, 1986; de Voogd et al., 1986, 1988; Russell and Snelson, 1994a). The COCORP data were acquired along profiles both transverse and parallel to the axis of the rift in the southern Albuquerque and northern Socorro Basins (Brown et al., 1980). Two transverse profiles are located on Figures 3 and 14 (New Mexico 1A and 1; also called Socorro 1A and Abo Pass 1). Various reprocessed time sections and an even greater variety of interpretations of crustal structure have resulted from the previous work. The greatest differences are for the west half of line 1A (vibration point [VP] locations northwest of VP200; Fig. 14).

Figure 14 compares our initial and final 3D models to COCORP line 1A in plan and cross-section view. In plan view, line 1A is located on an elevation contour map derived from the final 3D geophysical model. In cross-section view, curves extracted from the initial and final 3D thickness model along the location of 1A are overlain on time and depth sections, respectively, and two previous interpretations (from Cape et al., 1983, and Russell and Snelson, 1994a). Cape et al. combined interpretation of seismic reflections with analysis of gravity and well data. The configuration of the Mesozoic–Paleozoic structural blocks east of VP200 in their model matches layers interpreted as pre-rift sedimentary rocks by de Voogd et al. (1988), who used synthetic seismic modeling. Russell and Snelson reinterpreted the COCORP line following their concepts from the seismic model for the whole basin, especially in comparison to nearby Shell line 52 (Fig. 14A).

Wu (1986), de Voogd et al. (1988), and Russell and Snelson (1994a) previously noted the problematic orientation of line 1A in relation to fault strike and geologic structure out of the plane of section. The problem is well demonstrated by the location of the line in relation to gradients in the structural elevation contour map from the 3D geophysical model (Fig. 14A). Line 1A partially follows the trend of a steep gradient in the model contour map as it wraps around the north and east side of the Ladron Mountains. The gradient likely represents the cumulative displacement along a series of major mapped faults (Fig. 1). Thus, the COCORP data image faults that dip and bend essentially in and out of the plane of section, allowing for variable results arising from different data-processing parameters and interpretations that are difficult to visualize in this orientation. Russell and Snelson (1994a) depicted this oblique view of structure by showing flat, folded extensional faults (Fig. 14D).

An overlay of the time-converted thickness values from the initial 3D gravity model on the seismic time section demonstrates how the 3D structure is imaged in 2D on the west half of line 1A (Fig. 14C). The 3D surface mimics seismic reflections and appears to have a shallow east dip from VP400 to VP300, whereas true dip is to the northeast. From about VP280 to VP210, both the seismic reflections and the model curve show an antiform that peaks under VP240. The antiform, which is much more

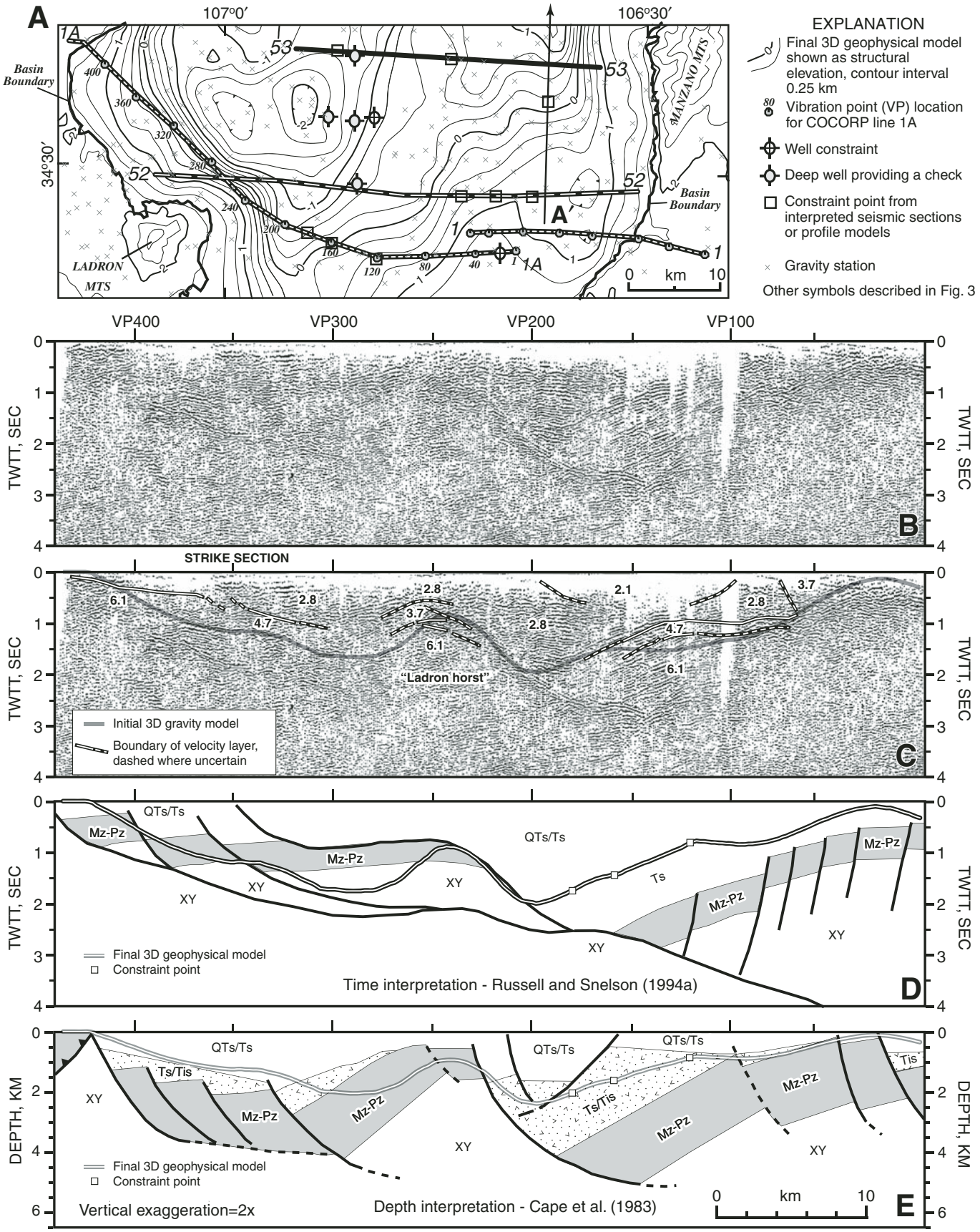

conspicuous on earlier versions of time sections (e.g., Brown et al., 1980, 1983), has been interpreted as the "Ladron horst." From the plan view of the 3D model (Fig. 14A), the "Ladron horst" extends west-northwest from the Ladron Mountains, appearing more as a plunging fold than a rift-related horst. Wu (1986) also noted this fold configuration and argued for a compressional origin; however, Lewis and Baldridge (1994) attributed the geometry solely to detachment-style faulting.

East of VP220, most of the previous seismic interpretations generally show west-dipping blocks that gradually gain in elevation on the east, with the west-dipping blocks corresponding to the prominent west-dipping reflections. Differences are in the interpretation of the geologic units composing the west-dipping blocks, as demonstrated by the differences in the Russell and Snelson (1994a) and Cape et al. (1983) models in Figure 14. Cape et al. (1983) interpreted Tertiary volcanic and sedimentary rocks (Ts/Tis on Fig. 14E) above a thick Mesozoic–Paleozoic section, whereas Russell and Snelson (1994a) interpreted a very thick Santa Fe Group section overlying a much thinner Mesozoic–Paleozoic section.

We instead interpret the base of the Santa Fe Group at the top of the prominent west-dipping reflections between VP200 and VP100. Points digitized along this boundary (constraint points marked on the model curve for Fig. 14D and 14E) were used to constrain the final 3D geophysical model. The top of the prominent west-dipping reflections corresponds to the top of a 4.7 km/sec velocity layer interpreted by Jurdy and Brocher (1980) between VP160 and VP60 (Fig. 14C). A velocity of 4.7 km/sec is too high to reasonably represent the Santa Fe Group (Table 2; Brocher, 1981), so this layer must represent older rocks or volcanic rocks. The initial 3D model curve coincides with the top of these reflections between VP200 and V170, but dips below the 4.7 km/s layer between VP160 and VP60. The dip may be partially caused by the sparse gravity data coverage in this area just to the north of line 1A (Fig. 14A). In general, poor data coverage in a north-south swath from VP160–VP100 on line 1A on the south to line 53 on the north results in poor representation of gradients in the model, despite the good constraints from well and seismic data. In short, we argue for a Neogene rift basin that reaches ~2 km depth in this area versus one that is ~4 km (>12,000 ft) deep, as depicted in the Russell-Snelson model (Fig. 2B).

Figure 14. Comparison of three-dimensional (3D) model results with Consortium for Continental Reflection Profiling (COCORP) line 1A in plan view (A) and cross-section view (B–E). Cross sections use vibration point (VP) locations along line 1A for reference and are plotted at a different scale than the plan view. Geologic codes in D and E are the same as Figure 1. (A) Plan view showing contours of elevation above sea level on the base of Santa Fe Group from the final 3D geophysical model and locations of COCORP lines. The western half of COCORP line 1A closely follows a prominent gradient in the 3D model near the Coyote fault (Fig. 1). Thus, both velocity analysis and position of reflection surfaces on this part of the seismic section are ambiguous, because energy may be coming from either updip or downdip out of the section. (B) Unmigrated time section for line 1A from Russell and Snelson (1994a). TWTT—two-way travel time. Processing details and arguments against migrating the section are given by de Voogd et al. (1988). (C) The same time section overlain by a time-converted curve extracted from the initial 3D gravity model and velocity layers from the refraction analysis of Jurdy and Brocher (1980). (D) Line drawing of the interpreted time section of Russell and Snelson (1994a) overlain by the time-converted curve from the final 3D geophysical model, showing the location of constraint points. (E) Line drawing of the interpreted depth section of Cape et al. (1983) overlain by a curve extracted from the final 3D geophysical model, showing the location of constraint points.

DISCUSSION

The final 3D geophysical model shows variations in rift-fill thickness that provide a new perspective on basin geometry compared to previous models, especially for the southern Albuquerque Basin. The model provides revised information for developing regional groundwater models, assessing seismic hazards, and exploring for energy resources. In this section, we discuss how the geophysical model additionally can be used to investigate the subsidence history and internal structure of the basin, as well as delineate major accommodation zones, suggest areas to investigate buried pre-rift structure and early-rift strata, and pose possible scenarios for the distribution of coarse-grained sediments within the basin-fill aquifer.

Subsidence History

To better understand the origins of the basin geometry indicated by the 3D geophysical model, we first identify major half grabens indicated by the model then look at evidence for subsidence history of each of these. As illustrated by the model shown in the inset on Figure 15, half grabens within rift basins are generally recognized next to their boundary faults by (1) pronounced asymmetry in isopach or structural elevation contours that have a semi-ellipsoidal shape in map view, (2) basin floors that are broadly synclinal in longitudinal section, and (3) depositional layers that fan toward the fault as a wedge in cross section (e.g., Rosendahl, 1987; Schlische and Anders, 1996; Morley, 1999, 2002). Using these criteria, several half grabens are identified and shown schematically in Figure 15: the "Calabacillas half graben," which covers most of the Calabacillas subbasin; and the Hubbell, Mountainview, and Coyote half grabens, which are isolated from each other within the Belen subbasin. The Coyote half graben is speculative because it is recognized only by the first two of the criteria.

One might expect the north-trending Calabacillas and Hubbell half grabens and the northwest-trending, oppositely tilted Coyote and Mountainview half grabens to have similar subsidence histories, because of their similar trends. However, age relations support similar rapid-uplift histories for the Calabacillas and Coyote half grabens and somewhat different, long-lived histories for the Mountainview and Hubbell half grabens. Subsidence of the Calabacillas and Coyote half grabens was apparently

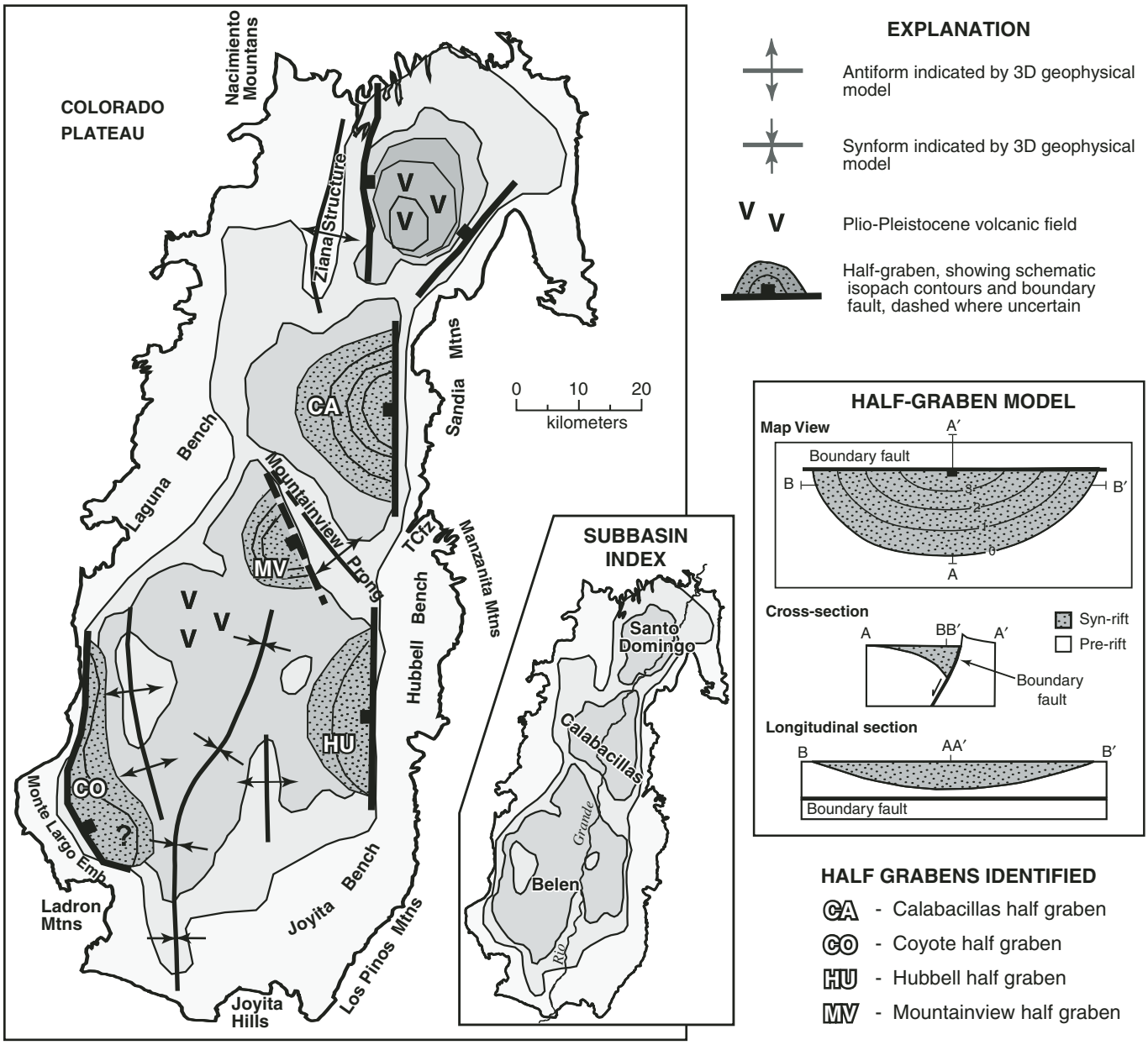

Figure 15. Schematic diagram depicting subbasin outlines, half grabens, and intrabasinal structures identified in the three-dimensional (3D) geophysical model (Fig. 6). The subbasins are generally outlined by the 1 km and 2 km isopach contours of the final 3D geophysical model (Fig. 5B). Half grabens were identified following the model shown, derived from models of boundary-fault propagation with associated depocenter development and footwall uplift from Schlische and Anders (1996), Morley (1999), Ebinger et al. (1999), and Morley (2002). Numbers and contours on the map view of the half-graben model represent contours of structural elevation of the basin floor in kilometers.

synchronous and fairly rapid during middle Miocene time. This conclusion is based on evidence for Miocene cooling and uplift of the Sandia Mountains in the northeast and the Ladron Mountains in the southwest from apatite and zircon fission-track data, the sedimentary record, geomorphology of uplifted scarps, and flexural models (Kelley, 1977; Lozinsky and Tedford, 1991; Kelley et al., 1992; Lewis and Baldridge, 1994; May et al., 1994; Roy et al., 1999; Connell, 2008b; Connell et al., this volume). Some of these authors attributed the rapid uplift to footwall unloading, in the style proposed by Wernicke and Axen (1988).

Although the Mountainview half graben is not evident from regional geologic mapping (Maldonado et al., 1999, 2007), subsurface data suggest it was active throughout most of rift history. May and Russell (1994) conclude that subsidence of the Mountainview half graben began toward the end of Oligocene time, culminating in 533 m of Oligocene unit of Isleta #2 and 4407 m of undivided

Santa Fe Group (Lozinsky, 1994) deposited at the site of the Shell 2 Isleta well (Fig. 3). Furthermore, a time-depth conversion (using velocities in Table 2) of May and Russell's tentative correlation of a 16.1 Ma basalt with reflections at 2.4 s TWTT on line 72 (Fig. 3) suggests that ~2.0 km of the sediments was deposited prior to 16 Ma and 2.9 km after. The half graben is at the northern end of a region of well-preserved petrocalcic soils that formed on a relict basin floor (Machette, 1985). Preservation of relict basin-floor surfaces and younger syn-rift fill across the Mountainview prong indicates that much of the footwall uplift occurred before Pliocene time. Plio-Pleistocene (<5 Ma) sediments and Upper Miocene (<8 Ma) volcanic rocks cover the area today (Maldonado et al., 2007; Connell, 2008b; Fig. 1), suggesting that the Mountainview half graben was inactive by Pleistocene time.

Previous workers have viewed the north-northwest orientation of the Mountainview prong (and associated boundary fault of the Mountainview half graben) to represent faulting within an earlier stress regime that eventually reoriented with time (Hudson et al., 2001). This scenario is compatible with the long history of rift-related deposition in the Mountainview half graben, the presence of both north-south and north-northwest fault trends near its eastern boundary (described in more detail in Appendix G), and evidence for tectonic rotation and reorientation of paleostress fields elsewhere near the study area (Hudson et al., 2001, 2007; Minor et al., this volume).

The age of formation of the Hubbell half graben is unclear, but it may also be a long-lived structural feature. Exposures of and unconformities between the Paleozoic and Mesozoic section, Paleogene rocks, and older and younger rift-basin fill indicate a long and complicated history of erosion and deposition on the Hubbell bench (Kelley, 1982; Connell et al., 2002), the footwall of the Hubbell half graben. On the basis of relations between apatite fission-track cooling ages, Kelley et al. (1992) suggested that the Hubbell bench was downfaulted from the Manzano Mountains into the basin after Eocene time. Geologic evidence suggests the faulting occurred prior to the late Oligocene, when much of the region was low relief and covered by volcanic rocks (Connell et al., 2002; Connell, 2004). Pleistocene activity of the Hubbell Spring fault is documented by evidence for large-magnitude earthquakes along prominent fault scarps (Personius and Mahan, 2003; Wong et al., 2004; Olig et al., 2011). Finally, a multi-stage history of activity on the Hubbell Spring fault zone is suggested by geophysical evidence. Gravity, magnetic, and magnetotelluric data all indicate the greatest vertical displacement related to the Hubbell Spring fault zone is located as much as 1 km west of the geomorphic scarp (Cordell, 1979; Grauch and Hudson, 2002; Rodriguez and Sawyer, this volume). The offset, which is not crossed by available seismic lines, is a robust feature of the 3D geophysical model (Figs. 6 and 12). In addition, high-resolution aeromagnetic data indicate a now-inactive normal fault that is 2–5 km east of the Hubbell Spring fault scarp (Grauch, 2001). Evidence of inactive faults on either side of the Quaternary Hubbell Spring fault scarp suggests that the locus of fault activity has shifted with time.

The overall eastward tilting of syn-rift strata in the Calabacillas subbasin (Fig. 9) does not support a model of late Miocene reversal of basin tilting, as proposed by Ingersoll (2001). In his model, the northern part of the Albuquerque Basin originally tilted to the west until late Miocene time, when the basin-fill strata began to tilt to the east in response to uplift along the eastern structural margin of the basin. If this model were to hold, stratal tilts near the base of the syn-rift succession should tilt to the west. Instead, overall eastward tilts at the base of the Santa Fe Group are supported by (1) the 3D geophysical model; (2) map patterns showing older Santa Fe Group along the western margin of the basin (Fig. 1); and (3) persistent, southeast-directed paleoflow indicators in Miocene–Plicoene fluvial deposits (e.g., Brandes, 2002). If such a reversal in polarity occurred, it may have happened during Oligocene time (Connell et al., 2007).

Accommodation Zones

The Tijeras transfer zone of the Russell-Snelson model (Fig. 2B) is described as a scissor-like, oblique-slip fault that accommodates the opposing tilts of north and south half-graben blocks within the Albuquerque Basin (Russell and Snelson, 1994a; May and Russell, 1994). Chapin and Cather (1994) speculated that northeast-striking transfer zones separating regions of opposing stratal tilt are characteristic of the central to northern Rio Grande rift, with or without attendant strike-slip displacement. Our 3D geophysical model does not support the accommodation of large, opposing half-graben blocks hypothesized for the Tijeras transfer zone, and does not show any obvious evidence for other northeast-striking transfer zones within the Albuquerque Basin. Instead, our model defines the northwest-trending Mountainview prong as the division between the northern (Calabacillas subbasin) and southern (Belen subbasin) parts of the Albuquerque Basin (Fig. 6). The position of the Mountainview prong between the en echelon north-trending Calabacillas and Hubbell half-graben boundary faults (Fig. 15) is similar to transverse anticlinal accommodation zones that might be expected in between two propagating boundary faults (Morley, 1999). However, the timing of fault propagation is not clear, as discussed above.

Instead of northeast-striking transfer zones, we find that Miocene strata of opposing dip are locally accommodated by faulted antiforms and a synform, such as the antiformal Mountainview prong and Ziana structure (Figs. 6 and 15) and multiple antiforms and a synform in the Belen subbasin (Fig. 12). The antiforms and synform in the Belen subbasin are not well expressed in overlying Plio-Pleistocene deposits (e.g., Maldonado et al., 1999, 2007), so they were likely formed during Miocene time. Antiforms and synforms commonly form in rift environments (Schlische, 1995; Morley et al., 1999a), and they may accommodate the propagation of overlapping or linking boundary faults (Rosendahl, 1987; Faulds and Varga, 1998).

The most far-reaching synform that accommodates opposing stratal tilts meanders from the southern tip of the Albuquerque Basin toward the Mountainview half graben (Figs. 6 and 15).

This synform may merge with the half graben on the north, but the intervening volcanic fields obscure the relations. Along profile C–C′ in the north-central part of the subbasin, the synform appears to be a local feature at the east side of broadly east-tilted strata (Fig. 12). At the far east of seismic line 81, strata appear to thicken to the east into this synform (Fig. 10). Along seismic line 53 in the south-central part of the Belen subbasin, the synform coincides with a depocenter, into which rift-fill strata both tilt and thicken (Fig. 11). At the southern tip of the basin, the synform is suggested by the converging dips of the reflections interpreted to underlie the Neogene rift fill and a slight curvature at the lowest point of the depocenter (about VP200 on Fig. 14). Thus, although the synform can be followed throughout the Belen subbasin, its nature varies, and its role in rifting is unclear.

An antiform that divides strata of opposing tilt in the southwest part of the Albuquerque Basin is partially aligned with the east-down Gabaldon fault (Kelley, 1977, 1979; Figs. 1 and 12). The antiform is best viewed in cross section in seismic line 81 (Fig. 10), where it divides a narrow, west-tilted half graben on the west from a broad, east-tilted half graben on the east. This faulted antiform is reminiscent of "inversion anticlines" identified in seismic lines from the East African rift that may have formed in response to a change in stress regime or reorganization of rift structures (Morley et al., 1999a, 1999b). In map view, the oblique orientation of the anticlinal axis in between the west-down Coyote fault and the buried, east-down Mountainview fault resembles the model of Faulds and Varga (1998) for an anticlinal, oblique antithetic accommodation zone. However, as discussed previously, these faults may not have been coeval.

The Ziana structure and the Laguna bench in the northwestern and western parts of the Albuquerque Basin, respectively, are prominent features in both the Russell-Snelson model (Fig. 2B) and our 3D geophysical model (Fig. 6). The Ziana structure is a fault-bounded, south-plunging anticline that is partially exposed (Black and Hiss, 1974; Kelley, 1977; Connell, 2008b). Previous workers have considered the structure as an anticlinal accommodation zone that forms the boundary between tilt domains (Stewart et al., 1998; Connell, 2004) or relays strain between the east-dipping northern Albuquerque and west-dipping southern Española Basins (May and Russell, 1994). The eastern edge of the Laguna bench is also evident from geologic mapping, generally along and/or east of the San Ysidro fault (SYf on Figs. 1 and 6). In contrast, the geophysically well-defined northeast-trending southern edge of the Laguna bench is not obvious at the surface (Fig. 1). This 30-km-long northeast-trending edge connects en echelon north-south segments of the western rift border (Figs. 6 and 15) in a way that broadly resembles a south-plunging relay ramp (or transfer zone) between the right-stepping border faults.

Pre-Rift Structure

The site of the Rio Grande rift experienced multiple tectonic events prior to Cenozoic rifting (Keller and Baldridge, 1999), so it should not be surprising to find evidence of older structures underlying the Albuquerque Basin. Many previous workers propose that pre-rift structures have controlled subsequent rift formation in the Rio Grande rift (e.g., Chapin and Seager, 1975; Cordell, 1976, 1978; Chapin, 1988; Cather, 1992; Russell and Snelson, 1994a; Kellogg, 1999; Karlstrom et al., 1999; Ingersoll, 2001). However, the importance of structural inheritance in rifts continues to be debated (e.g., Schlische and Withjack, 2008). We have recognized structures underlying the rift fill that may have Proterozoic, late Paleozoic Ancestral Rocky Mountain, or Cretaceous–Paleogene Laramide affinities. Some of these structures affect the overlying rift fill, and thus are expressed in the 3D geophysical model.

The prominent structural high under the Humble Shell Santa Fe #1 well on line 81 (Fig. 10) may be associated with the antiform at the base of the 3D geophysical model in the southwest part of the basin (Fig. 6). The structural high corresponds in part to a large magnetic anomaly that appears to be basement related (Fig. 12), suggesting that basement heterogeneity has some influence on the structural development of the antiform and/or precursor structures. Alternatively, the basement high may have been an erosional remnant that acted as a nucleus for fault propagation (Schlische and Withjack, 2008).

The northwest boundary of the Joyita bench follows a north-northeast trend in the 3D geophysical model that parallels the strikes of shallow rift-age faults (Figs. 6 and 8). Previous workers have argued for a relation between these north-northeast rift-related faults, Proterozoic shear zones, and Laramide thrust and strike-slip faults exposed in the Manzano–Los Pinos Mountains and the Joyita Hills (Fig. 6; Beck and Chapin, 1994; Russell and Snelson, 1994a; Karlstrom et al., 2004). Low-angle reflections observed in crossing COCORP lines in the southeast part of the basin have been interpreted as a basinward extension of the Laramide Montosa thrust fault, which may have been reactivated as a rift-related detachment fault (de Voogd et al., 1986, 1988).

The north-south antiform in the geophysical model in the south-central part of the basin (Fig. 6) overlies the postulated Ancestral Rocky Mountains horst discussed in relation to seismic line 53 (Figs. 11 and 12). Previous workers have recognized north-south Ancestral Rocky Mountains horsts and grabens from exposed rocks in the Joyita Hills and the Nacimiento Mountains at the southern and northern extremes of the basin, respectively (Baars, 1982; Chapin, 1988; Beck and Chapin, 1994), and in the subsurface of the Estancia Basin just east of the Albuquerque Basin (Barrow and Keller, 1994; Broadhead, 1997) (Fig. 1). We speculate that other north-south antiforms in the model, such as the Mountainview prong and the Ziana structure, may also have Ancestral Rocky Mountains origins.

The Tijeras-Cañoncito fault appears to have a limited influence on variations in rift-fill thickness where it enters the basin on the east side (TCfz on Fig. 6)—not as substantial an influence as depicted by the Russell-Snelson model. As noted previously, the boundary faults of the Hubbell and Calabacillas half grabens are north-south, linear, and appear to be separated ~5 km in a right-lateral sense across the Tijeras-Cañoncito fault zone

(Fig. 15). Geologic evidence along the fault system supports more than 0.2 km of north-side-down vertical displacement at the basin margin, 0.5–2.4 km of left-lateral offset, and an unknown amount of earlier right-lateral movement (Kelley and Northrop, 1975; Abbott et al., 1995, 2004). Abbott et al. (2004) argued that the left-lateral movement occurred during rifting, whereas the right-lateral movement occurred during Laramide tectonic activity. However, a Laramide timing of right-lateral movement does not explain the right-lateral separation of rift boundary faults in the Albuquerque Basin. Either pre-rift structure has been reactivated or preserved, or the timing of the right-lateral slip needs to be reevaluated. On the north end of the Tijeras-Cañoncito fault system in the Española Basin, the pre-rift age of right-lateral movement is well established (Abbott et al., 2004; Lisenbee, this volume). Curiously, aeromagnetic anomalies likely caused by buried basement sources are offset ~5 km in a right-lateral sense along this northern part of the fault system (Grauch et al., 2009), similar to the amount of right-lateral separation observed in the Albuquerque Basin. These similarities suggest that the rift boundary faults in the Albuquerque Basin are following an older fault system that was earlier offset by Laramide tectonic activity.

It is unclear whether many of the pre-rift structures recognized in this study influenced rift formation or are merely preserved under the rift fill. Most have geophysical expressions that are difficult to separate from those that are rift-related without using multiple data sets, which might explain why previous interpretations of basin geometry have been so diverse. In any case, their presence should caution anyone involved in subsurface studies of the Rio Grande rift to be especially wary of confusing pre-rift versus rift structures.

Early-Rift Strata

Based on the characterization of densities (Fig. 4), which allows the 3D gravity inversion to separate rift fill from earlier sedimentary units, our modeling represents only the less-dense Miocene–Pleistocene deposits. Some strata imaged in the seismic sections below the modeled base of the Santa Fe Group may actually be older, early-rift deposits. For example, the west-dipping strata just below the model curve on the COCORP line between VP200 and VP120 (Fig. 14) fan toward the fault on the west, suggesting the deposition was syn-faulting (Cape et al., 1983). The relatively high velocities of these strata (4.7–6.1 km/s) are consistent with volcanic and volcaniclastic rocks that may correlate with 36–27 Ma eruptive units that crop out in the Socorro area to the south (Chamberlin, 1983; Cather et al., 1994). The lower parts of the west-dipping reflections may also include pre-rift, Oligocene Mogollon-Datil volcanic rocks, Eocene Baca Formation, as well as the Mesozoic–Paleozoic sedimentary section. Thus, some of the Mesozoic–Paleozoic section interpreted for COCORP line 1A by Cape et al. (1983; Fig. 14E), and some of the Santa Fe Group interpreted by Russell and Snelson (1994a; Fig. 14D) may represent a much thicker section of Paleogene rocks than previously interpreted.

Ancestral Rio Grande

The geometry and ages of component half grabens and accommodation zones are important because they control the distribution of sediment. For example, axial drainage tends to flow along the deeper portions of extensional basins (Gawthorpe and Leeder, 2000). The axial river of the Albuquerque Basin (the ancestral Rio Grande) deposited sands and gravels as early as late Miocene time that today compose a high-transmissivity facies within the basin aquifers. Thus, depocenters indicated by our 3D geophysical model can be used to postulate possible courses of the ancestral Rio Grande in between isolated stratigraphic constraints. These hypotheses can then help predict where high-transmissivity aquifers may be concealed.

Stratigraphic evidence indicates that the ancestral Rio Grande was established in the Santo Domingo subbasin by late Miocene time (Smith et al., 2001), but was not through-going south of the Belen subbasin until early Pliocene time (Connell et al., 2005; Mack et al., 2006). The former courses of the ancestral Rio Grande are evident by axial-river deposits mapped on both sides of the Santo Domingo subbasin (Smith et al., 2001), near the eastern edge of the east-tilted Calabacillas subbasin (Connell, 2008b), and along the southwestern edge of the Belen subbasin (Machette, 1978; Connell and McCraw, 2007). These areas coincide with deep parts of the 3D geophysical model next to basin boundaries, suggesting that this axial river followed structural depressions in the basin (Gawthorpe and Leeder, 2000). South of axial-fluvial deposit exposures in the Calabacillas subbasin, the ancestral Rio Grande probably flowed into the Belen subbasin along either the west or east side of the Mountainview prong. The overall lack of ancestral Rio Grande sediments exposed west of the Rio Grande (Maldonado et al., 2007; Connell et al., this volume) suggests that the axial river probably flowed closer to the Hubbell Spring fault zone (and across the eastern side of the Mountainview prong) rather than through the Mountainview half graben. In the Belen subbasin, the earlier river course may have followed the alignment of the central synform expressed in the 3D geophysical model to reach the southern part of the basin, where axial-fluvial deposits are exposed in fault-bounded blocks along the eastern flank of the Ladron Mountains (e.g., Machette, 1978).

CONCLUSIONS

An improved view of the structure and geometry of the Albuquerque Basin can be achieved through the integration and joint interpretation of various geological and geophysical data sets. A 3D geophysical model of basin-fill thickness was developed for the Albuquerque Basin, one of the largest structural basins of the Rio Grande rift. This model capitalized on a natural separation between the density of syn-rift sediments of the Santa Fe Group and those of older rocks. This model used a 3D gravity inversion that was constrained by seismic-reflection data, geologic cross sections, well information, and 2D forward models of selected

cross sections, to produce a geophysical model to examine the structure and tectonic development of the Albuquerque Basin in north-central New Mexico.

The geometry of the Albuquerque Basin is primarily a result of Miocene subsidence that led to the formation of three interconnected structural depressions that increase in size and complexity to the south. These structural subbasins, divided by narrow structural ridges, are (from north to south): the Santo Domingo, Calabacillas, and Belen subbasins. The subbasins are flanked by structural benches on east and west sides that range in width from 5 to 25 km. The northern Santo Domingo subbasin is fairly symmetric, with a north-south boundary on the west side and a northeast-trending boundary on the southeast side. The central Calabacillas subbasin is a large, asymmetric, east- to northeast-tilted half graben deepening to 4–5 km. The southern Belen subbasin is a composite of elongated ridges and troughs of varying asymmetry, with basin fill ranging from 3 to 5 km thick. The subbasin floor predominantly tilts broadly eastward, whereas steeper, west to southwest tilts are generally restricted to the southwestern part of the subbasin. The southward increase in complexity of the subbasins may reflect a transition from the topographically and structurally well-defined Rio Grande rift in northern New Mexico and southern Colorado, to rifting within a broader region of crustal extension within the Basin and Range province.

The 3D geophysical model indicates that the three subbasins can be further subdivided into smaller half-graben segments and synformal and antiformal features that strongly influence basin structure and the basin-fill thickness. Accommodation zones are represented by antiforms and a synform where opposing stratal tilts come together. Three distinct half grabens are identified within the Belen subbasin, two of which appear to have had a long-lived rift history.

The 3D geophysical model provides new perspectives on basin geometry that differ from a widely accepted structural model based primarily on seismic-reflection interpretations (Russell and Snelson, 1994a). A key improvement to earlier structural models is the lack of evidence for the Rio Grande fault and Tijeras transfer zone. The eastern rift border is located as much as 20 km east of the Rio Grande fault of Russell and Snelson (1994a). Geophysical and geologic mapping evidence for a discrete, southwest-trending, scissor-like Tijeras transfer zone is not well supported. Rather than a discrete structural zone that separates predominantly east-tilted strata in the Calabacillas subbasin from predominantly west-tilted strata to the south, the overall change in stratal tilts tends to be rather complicated in the Belen subbasin.

The basin geometry depicted by the 3D geophysical model has important implications for tectonic and sedimentation history. The slopes of the basin floor depicted by the 3D geophysical model generally conform to stratal tilts at the base of the Santa Fe Group evident from seismic data and mapped bedding attitudes in the Calabacillas and northern Belen subbasins. The overall eastward tilts, except in the southwestern part of the basin, support geologic evidence for a prolonged history of eastward tilt during Miocene deposition. A central axial synform in the Belen subbasin suggests a possible path for the ancestral Rio Grande during late Miocene to Pliocene time, providing a rationale for predicting where coarse-grained axial-river deposits may be buried within the basin fill. Finally, variations in basin-fill thickness coincide with earlier structures in several places, suggesting that pre-rift structures have had a role in rift development.

ACKNOWLEDGMENTS

We are indebted to John J. Miller (USGS), who reprocessed the digital seismic data and prepared information for Appendix B, and David Sawyer (USGS), who helped gather and compile well information at the beginning of the project. David Taylor (USGS, deceased) was instrumental in the original acquisition of digital seismic data from Seismic Exchange, Inc. (SEI). We publish these data with permission from SEI. We are grateful for insightful feedback provided by Bruce Black and Brian Brister and helpful discussions at different stages in the development of the model with Ron Broadhead, Steve Cather, Richard Chamberlin, John Hawley, Mark Hudson, Randy Keller, Dan Koning, Dave Love, Scott Minor, and Brian Rodriguez. This contribution was supported by the USGS National Cooperative Geologic Mapping Program and the New Mexico Bureau of Geology and Mineral Resources. Any use of trade names is for descriptive purposes only and does not imply endorsement by the U.S. Government.

REFERENCES CITED

Abbott, J.C., Cather, S.M., and Goodwin, L.B., 1995, Paleogene synorogenic sedimentation in the Galisteo basin related to the Tijeras-Cañoncito fault system, *in* Goff, F., Kues, B.S., Rogers, M.A., McFadden, L.D., and Gardner, J.N., eds., Jemez Mountains Region: New Mexico Geological Society Guidebook 46, p. 271–278.

Abbott, J.C., Goodwin, L.B., Kelley, S.A., Maynard, S.R., and McIntosh, W.C., 2004, The anatomy of a long-lived fault system—Structural and thermochronologic evidence for Laramide to Quaternary activity on the Tijeras fault, New Mexico, *in* Cather, S.M., McIntosh, W.C., and Kelley, S.A., eds., Tectonics, Geochronology, and Volcanism in the Southern Rocky Mountains and Rio Grande Rift: New Mexico Bureau of Geology and Mineral Resources Bulletin 160, p. 113–138.

Baars, D.L., 1982, Paleozoic history of the Albuquerque trough: Implications of basement control on Rio Grande rift, *in* Grambling, J.A., Wells, S.G., and Callender, J.F., eds., Albuquerque Country II: New Mexico Geological Society Guidebook 33, p. 153–157.

Baldridge, W.S., Keller, G.R., Haak, V., Wendlandt, E., Jiracek, G.R., and Olsen, K.H., 1995, The Rio Grande rift, *in* Olsen, K.H., ed., Continental Rifts: Evolution, Structure, and Tectonics: Developments in Tectonics 25: Amsterdam, Elsevier Publishing Company, p. 233–275.

Barrow, R., and Keller, G.R., 1994, An integrated geophysical study of the Estancia Basin, central New Mexico, *in* Keller, G.R., and Cather, S.M., eds., Basins of the Rio Grande Rift: Structure, Stratigraphy, and Tectonic Setting: Geological Society of America Special Paper 291, p. 171–186.

Bartolino, J.R., and Cole, J.C., 2002, Ground-Water Resources of the Middle Rio Grande Basin, New Mexico: U.S. Geological Survey Circular 1222, 132 p.

Beck, W.C., and Chapin, C.E., 1994, Structural and tectonic evolution of the Joyita Hills, central New Mexico: Implications of basement control on Rio Grande rift, *in* Keller, G.R., and Cather, S.M., eds., Basins of the Rio Grande Rift: Structure, Stratigraphy, and Tectonic Setting: Geological Society of America Special Paper 291, p. 187–205.

Birch, F.S., 1982, Gravity models of the Albuquerque basin, Rio Grande rift, New Mexico: Geophysics, v. 47, p. 1185–1197.

Black, B.A., 1982, Oil and gas exploration in the Albuquerque basin, *in* Grambling, J.A., Wells, S.G., and Callender, J.F., eds., Albuquerque Country II: New Mexico Geological Society Guidebook 33, p. 313–324.

Black, B.A., 1999, Recent oil and gas exploration in the Albuquerque basin, *in* Pazzaglia, F.J., and Lucas, S.G., eds., Albuquerque Geology: New Mexico Geological Society Guidebook 50, p. 437–440.

Black, B.A., and Hiss, W.L., 1974, Structure and stratigraphy in the vicinity of the Shell Oil Co. Santa Fe Pacific No. 1 test well, Southern Sandoval County, New Mexico, *in* Siemers, C.T., Woodward, L.A., and Callender, J.F., eds., Ghost Ranch: New Mexico Geological Society Guidebook 25, p. 365–370.

Blakely, R.J., 1995, Potential Theory in Gravity and Magnetic Applications: Cambridge, UK, Cambridge University Press, 441 p.

Bott, M.H.P., 1960, The use of rapid digital computing methods for direct gravity interpretation of sedimentary basins: Geophysical Journal, v. 3, p. 63–67, doi:10.1111/j.1365-246X.1960.tb00065.x.

Bott, M.H.P., and Hinze, W.J., 1995, Potential field methods, *in* Olsen, K.H., ed., Continental Rifts: Evolution, Structure, Tectonics: Developments in Geotectonics 25: Amsterdam, Elsevier Publishing Company, p. 93–101.

Brandes, N.N., 2002, Lithostratigraphy and Petrography of Upper Santa Fe Group Deposits in the Northern Albuquerque Basin, New Mexico [M.S. thesis]: Socorro, New Mexico Institute of Mining and Technology, 208 p.

Broadhead, R.F., 1997, Subsurface geology and oil and gas potential of Estancia Basin, New Mexico: New Mexico Bureau of Mines and Mineral Resources Bulletin 157, 54 p.

Broadhead, R.F., 2009, Oil and natural gas potential of the Albuquerque Basin, *in* Price, L.G., Bland, D., Johnson, P.S., and Connell, S.D., eds., Water, Natural Resources, and the Urban Landscape—The Albuquerque Region: New Mexico Bureau of Geology and Mineral Resources Decision-Makers Field Conference 2009, p. 80–86.

Brocher, T.M., 1981, Shallow velocity structure of the Rio Grande rift north of Socorro, New Mexico: A reinterpretation: Journal of Geophysical Research, v. 86, p. 4960–4970, doi:10.1029/JB086iB06p04960.

Brown, L.D., Krumhansl, P.A., Chapin, C.E., Sanford, A.R., Cook, F.A., Kaufman, S., Oliver, J.E., and Schilt, F.S., 1979, COCORP seismic reflection studies of the Rio Grande rift, *in* Riecker, R.E., ed., Rio Grande Rift: Tectonics and Magmatism: Washington, D.C., American Geophysical Union, p. 169–184.

Brown, L.D., Chapin, C.E., Sanford, A.R., Kaufman, S., and Oliver, J., 1980, Deep structure of the Rio Grande rift from seismic reflection profiling: Journal of Geophysical Research, v. 85, p. 4773–4800, doi:10.1029/JB085iB09p04773.

Brown, L.D., Kaufman, S., and Oliver, J.E., 1983, COCORP seismic traverse across the Rio Grande rift, *in* Bally, A.W., ed., Seismic Expression of Structural Styles: A Picture and Work Atlas: American Association of Petroleum Geologists Studies in Geology 15, v. 2, p. 2.1.1–2.1.6.

Cabezas, P., 1991, The southern Rocky Mountains in west-central New Mexico—Laramide structures and their impact on the Rio Grande rift extension: New Mexico Geology, v. 13, p. 25–37.

Callender, J.F., and Zilinski, R.E., 1976, Kinematics of Tertiary and Quaternary deformation along the eastern edge of the Lucero uplift, central New Mexico, *in* Woodward, L.A., and Northrup, S.A., eds., Tectonics and Mineral Resources of Southwestern North America: New Mexico Geological Society Special Publication 6, p. 53–71.

Cape, C.D., McGeary, S., and Thompson, G.A., 1983, Cenozoic normal faulting and the shallow structure of the Rio Grande rift near Socorro, New Mexico: Geological Society of America Bulletin, v. 94, p. 3–14, doi:10.1130/0016-7606(1983)94<3:CNFATS>2.0.CO;2.

Cather, S.M., 1992, Suggested revisions to the Tertiary tectonic history of north-central New Mexico, *in* Lucas, S.G., Kues, B.S., Williamson, T.E., and Hunt, A.P., eds., San Juan Basin IV: New Mexico Geological Society Guidebook 43, p. 109–122.

Cather, S.M., 2004, Laramide orogeny in central and northern New Mexico and southern Colorado, *in* Mack, G.H., and Giles, K.A., eds., The Geology of New Mexico: New Mexico Geological Society Special Publication 11, p. 203–248.

Cather, S.M., Chamberlin, R.M., Chapin, C.E., and McIntosh, W.C., 1994, Stratigraphic consequences of episodic extension in the Lemitar Mountains, central Rio Grande rift, *in* Keller, G.R., and Cather, S.M., eds., Basins of the Rio Grande Rift: Structure, Stratigraphy, and Tectonic Setting: Geological Society of America Special Paper 291, p. 157–170.

Chamberlin, R.M., 1983, Cenozoic domino-style crustal extension in the Lemitar Mountains, New Mexico: A summary, *in* Chapin, C.E., and Callender, J.F., eds., Socorro Region II: New Mexico Geological Society Guidebook 34, p. 111–118.

Chapin, C.E., 1988, Axial basins of the northern and central Rio Grande rift, *in* Sloss, L.L., ed., Sedimentary Cover—North American Craton: Boulder, Colorado, Geological Society of America, Geology of North America, v. D-2, p. 165–170.

Chapin, C.E., and Cather, S., 1994, Tectonic setting of the axial basins of the northern and central Rio Grande rift, *in* Keller, G.R., and Cather, S.M., eds., Basins of the Rio Grande Rift: Structure, Stratigraphy, and Tectonic Setting: Geological Society of America Special Paper 291, p. 5–23.

Chapin, C.E., and Seager, W.R., 1975, Evolution of the Rio Grande rift in the Socorro and Las Cruces areas, *in* Lucas, S.G., and Zidek, J., eds., Santa Rosa–Tucumcari Region: New Mexico Geological Society Guidebook 36, p. 297–321.

Chapin, C.E., McIntosh, W.C., and Chamberlin, R., 2004, The late Eocene–Oligocene peak of Cenozoic volcanism in southwestern New Mexico, *in* Mack, G.H., and Giles, K.J., eds., The Geology of New Mexico, A Geologic History: New Mexico Geological Society Special Publication 11, p. 271–293.

Connell, S.D., 2004, Geology of the Albuquerque Basin and tectonic development of the Rio Grande rift, north-central New Mexico, *in* Mack, G.H., and Giles, K.J., eds., The Geology of New Mexico, A Geologic History: New Mexico Geological Society Special Publication 11, p. 359–388.

Connell, S.D., 2006, Preliminary Geologic Map of the Albuquerque–Rio Rancho Metropolitan Area and Vicinity, Bernalillo and Sandoval County, New Mexico: New Mexico Bureau of Geology and Mineral Resources Open-File Report 496, version 2.0, CD-ROM.

Connell, S.D., 2008a, Refinements to the stratigraphic nomenclature of the Santa Fe Group, northwestern Albuquerque Basin, New Mexico: New Mexico Geology, v. 30, p. 14–35.

Connell, S.D., 2008b, Geologic Map of the Albuquerque–Rio Rancho Metropolitan Area, Bernalillo and Sandoval County, New Mexico: New Mexico Bureau of Geology and Mineral Resources Geologic Map GM-78, scale 1:50,000, 2 pls.

Connell, S.D., and McCraw, D.J., 2007, Preliminary Geologic Map of the La Joya NW Quadrangle, Socorro County, New Mexico: New Mexico Bureau of Geology and Mineral Resources Open-File Geologic Map 140, scale 1:24,000.

Connell, S.D., and Wells, S.G., 1999, Pliocene and Quaternary stratigraphy, soils, and tectonic geomorphology of the northern flank of the Sandia Mountains, New Mexico: Implications for the tectonic evolution of the Albuquerque basin, *in* Pazzaglia, F.J., and Lucas, S.G., eds., Albuquerque Geology: New Mexico Geological Society Guidebook 50, p. 379–391.

Connell, S.D., Allen, B.D., and Hawley, J.W., 1998, Subsurface stratigraphy of the Santa Fe Group using borehole geophysical logs, Albuquerque area, central New Mexico: New Mexico Geology, v. 20, p. 2–7.

Connell, S.D., McIntosh, W.C., and Rogers, S., 2002, Geology of Trigo Canyon, Valencia County, New Mexico—Uplift constraints for the southern Manzano Mountains [abstract]: New Mexico Geology, v. 24, p. 60.

Connell, S.D., Hawley, J.W., and Love, D.W., 2005, Late Cenozoic drainage development in the southeastern Basin and Range of New Mexico, southeasternmost Arizona, and western Texas, *in* Lucas, S.G., Morgan, G.S., and Ziegler, K.E., eds., New Mexico's Ice Ages: New Mexico Museum of Natural History and Science Bulletin 28, p. 125–150.

Connell, S.D., Koning, D.J., Kelley, S.A., and Brandes, N.N., 2007, Oligocene–Miocene sedimentation in the southwestern Jemez Mountains and northwestern Albuquerque basin, New Mexico, *in* Kues, B.S., Kelley, S.A., and Lueth, V.W., eds., Geology of the Jemez Region II: New Mexico Geological Society Guidebook 58, p. 195–208.

Connell, S.D., Smith, G.A., Geissman, J.W., and McIntosh, W.C., 2013, this volume, Climatic controls on nonmarine depositional sequences in the Albuquerque Basin, Rio Grande rift, north-central New Mexico, *in* Hudson, M.R., and Grauch, V.J.S., eds., New Perspectives on Rio Grande Rift Basins: From Tectonics to Groundwater: Geological Society of America Special Paper 494, doi:10.1130/2013.2494(15).

Cordell, L., 1976, Aeromagnetic and gravity studies of the Rio Grande graben in New Mexico between Belen and Pilar, *in* Woodward, L.A., and Northrup, S.A., eds., Tectonics and Mineral Resources of Southwestern North America: New Mexico Geological Society Special Publication 6, p. 62–70.

Cordell, L., 1978, Regional geophysical setting of the Rio Grande rift: Geological Society of America Bulletin, v. 89, p. 1073–1090, doi:10.1130/0016-7606(1978)89<1073:RGSOTR>2.0.CO;2.

Cordell, L., 1979, Sedimentary facies and gravity anomaly across master faults of the Rio Grande rift in New Mexico: Geology, v. 7, p. 201–205, doi:10.1130/0091-7613(1979)7<201:SFAGAA>2.0.CO;2.

Crumpler, L.S., 1999, Ascent and eruption at the Albuquerque volcanoes: A physical volcanology perspective, *in* Pazzaglia, F.J., and Lucas, S.G., eds., Albuquerque Geology: New Mexico Geological Society Guidebook 50, p. 221–233.

de Voogd, B., Brown, L.D., and Merey, C., 1986, Nature of the eastern boundary of the Rio Grande rift from COCORP surveys in the Albuquerque basin, New Mexico: Journal of Geophysical Research, v. 91, p. 6305–6320, doi:10.1029/JB091iB06p06305.

de Voogd, B., Serpa, L., and Brown, L.D., 1988, Crustal extension and magmatic processes, COCORP profiles from Death Valley and the Rio Grande rift: Geological Society of America Bulletin, v. 100, p. 1550–1567, doi:10.1130/0016-7606(1988)100<1550:CEAMPC>2.3.CO;2.

Drenth, B.J., Grauch, V.J.S., and Rodriguez, B.D., 2013, this volume, Geophysical constraints on Rio Grande rift structure in the central San Luis Basin, Colorado and New Mexico, *in* Hudson, M.R., and Grauch, V.J.S., eds., New Perspectives on Rio Grande Rift Basins: From Tectonics to Groundwater: Geological Society of America Special Paper 494, doi:10.1130/2013.2494(04).

Ebinger, C.J., Jackson, J.A., Foster, A.N., and Hayward, N.J., 1999, Extensional basin geometry and the elastic lithosphere: Philosophic Transactions of the Royal Society of London, ser. A, v. 357, p. 741–765.

Faulds, J.E., and Varga, R.J., 1998, The role of accommodation zones and transfer zones in the regional segmentation of extended terranes, *in* Faulds, J.E., and Stewart, J.H., eds., Accommodation Zones and Transfer Zones: The Regional Segmentation of the Basin and Range Province: Geological Society of America Special Paper 323, p. 1–45.

Ferguson, J.F., Felch, R.N., Aiken, C.L.V., Oldow, J.S., and Dockery, H., 1988, Models of the Bouguer gravity and geologic structure at Yucca Flat, Nevada: Geophysics, v. 53, p. 231–244.

Foster, R.W., 1978, Selected data for deep drill holes along the Rio Grande rift, *in* Hawley, J.W., ed., Guidebook to the Rio Grande Rift in New Mexico and Colorado: New Mexico Bureau of Mines and Mineral Resources Circular 163, p. 236–237.

Gardner, G.H.F., Gardner, L.W., and Gregory, A.R., 1974, Formation velocity and density—The diagnostic basics for stratigraphic traps: Geophysics, v. 39, p. 770–780.

Gawthorpe, R.L., and Leeder, M.R., 2000, Tectono-sedimentary evolution of active extensional basins: Basin Research, v. 12, p. 195–218, doi:10.1046/j.1365-2117.2000.00121.x.

Gillespie, C.L., 2002, Integrated Geophysical, Geological and Remote Sensing Study of Selected Basins in the Rio Grande Rift [Ph.D. thesis]: El Paso, University of Texas at El Paso, 184 p.

Gillespie, C.L., Grauch, V.J.S., Oshetski, K., and Keller, G.R., 2000, Principal Facts for Gravity Data Collected in the Southern Albuquerque Basin and a Regional Compilation, Central New Mexico: U.S. Geological Survey Open-File Report 00-490, digital data available from http://pubs.usgs.gov/of/2000/ofr-00-0490/.

Goff, F., and Gardner, J.N., 2004, Late Cenozoic geochronology of volcanism and mineralization in the Jemez Mountains and Valles caldera, north central New Mexico, *in* Mack, G.H., and Giles, K.J., eds., The Geology of New Mexico, A Geologic History: New Mexico Geological Society Special Publication 11, p. 295–311.

Grauch, V.J.S., 1999, Principal features of high-resolution aeromagnetic data collected near Albuquerque, New Mexico, *in* Pazzaglia, F.J., and Lucas, S.G., eds., Albuquerque Geology: New Mexico Geological Society Guidebook 50, p. 115–118.

Grauch, V.J.S., 2001, High-resolution aeromagnetic data, a new tool for mapping intrabasinal faults: Example from the Albuquerque basin, New Mexico: Geology, v. 29, p. 367–370, doi:10.1130/0091-7613(2001)029<0367:HRADAN>2.0.CO;2.

Grauch, V.J.S., and Hudson, M.R., 2002, Implications of significant distances between major faults and large vertical displacements based on geophysical evidence, central Rio Grande rift, New Mexico: Geological Society of America Abstracts with Programs, v. 34, no. 6, p. 452.

Grauch, V.J.S., and Hudson, M.R., 2007, Guides to understanding the aeromagnetic expression of faults in sedimentary basins: Lessons learned from the central Rio Grande rift, New Mexico: Geosphere, v. 3, p. 596–623, doi:10.1130/GES00128.1.

Grauch, V.J.S., Gillespie, C.L., and Keller, G.R., 1999, Discussion of new gravity maps for the Albuquerque basin area, *in* Pazzaglia, F.J., and Lucas, S.G., eds., Albuquerque Geology: New Mexico Geological Society Guidebook 50, p. 119–124, 2 pls.

Grauch, V.J.S., Sawyer, D.A., Hudson, M.R., Minor, S.A., and Thompson, R.A., 2006, Gravity and aeromagnetic studies in the Santo Domingo basin area, *in* Minor, S.A., ed., The Cerrillos Uplift, the La Bajada Constriction, and Hydrogeologic Framework of the Santo Domingo Basin, Rio Grande Rift, New Mexico: U.S. Geological Survey Professional Paper 1720-D, p. 63–86.

Grauch, V.J.S., Phillips, J.D., Koning, D.J., Johnson, P.S., and Bankey, V., 2009, Geophysical Interpretations of the Southern Española Basin, New Mexico, That Contribute to Understanding Its Hydrogeologic Framework: U.S. Geological Survey Professional Paper 1761, 88 p., http://pubs.usgs.gov/pp/1761/.

Hansen, R.O., and Simmonds, M., 1993, Multiple-source Werner deconvolution: Geophysics, v. 58, p. 1792–1800.

Hawley, J.W., 1996, Hydrogeologic Framework of Potential Recharge Areas in the Albuquerque Basin, Central New Mexico, *in* Hawley, J.W., and Whitworth, T.M., compilers, Hydrogeology of Potential Recharge Areas for the Basin- and Valley-Fill Aquifer Systems, and Hydrogeochemical Modelling of Proposed Artificial Recharge of the Upper Santa Fe Aquifer, Northern Albuquerque Basin, New Mexico: New Mexico Bureau of Mines and Mineral Resources Open-File Report 402-D, p. 1–68.

Heywood, C.E., 1992, Isostatic Residual Gravity Anomalies of New Mexico: U.S. Geological Survey Water-Resources Investigations Report 91-4065, 27 p.

Hudson, M.R., and Grauch, V.J.S., 2003, Paleomagnetic evidence for a Tertiary not Triassic age for rocks in the lower part of the Grober-Fuqua #1 well, southeastern Albuquerque Basin, New Mexico: New Mexico Geology, v. 25, p. 31–36.

Hudson, M.R., Minor, S.A., and Grauch, V.J.S., 2001, Fault framework for the Albuquerque basin, Rio Grande rift: Geological Society of America Abstracts with Programs, v. 33, no.5, p. A-47.

Hudson, M.R., Minor, S.A., Thompson, R.A., Caine, J.S., and Brown, L.L., 2007, Pliocene strain transfer in the Rio Grande rift of north-central New Mexico: Geological Society of America Abstracts with Programs, v. 39, no. 6, p. 495.

Hudson, M.R., Grauch, V.J.S., and Minor, S.A., 2008, Rock magnetic characterization of faulted sediments with associated magnetic anomalies in the Albuquerque basin, Rio Grande rift, New Mexico: Geological Society of America Bulletin, v. 120, p. 641–658, doi:10.1130/B26213.1.

Ingersoll, R.V., 2001, Structural and stratigraphic evolution of the Rio Grande rift, northern New Mexico and southern Colorado: International Geology Review, v. 43, p. 867–891, doi:10.1080/00206810109465053.

Ingersoll, R.V., 2003, Structural and stratigraphic evolution of the Rio Grande rift, northern New Mexico and southern Colorado, *in* Klemperer, S.L., and Ernst, W.G., eds., The Lithosphere of Western North America and Its Geophysical Characterization: The George A. Thompson Volume, International Book Series 7: Columbia, Maryland, Bellwether Publishing for the Geological Society of America, p. 251–275.

Jachens, R.C., and Moring, B.C., 1990, Maps of the Thickness of Cenozoic Deposits and the Isostatic Residual Gravity over Basement for Nevada: U.S. Geological Survey Open-File Report 90-404, 15 p., http://pubs.er.usgs.gov/usgspubs/ofr/ofr90404.

Jachens, R.C., Moring, B.C., and Schruben, P.G., 1996, Thickness of Cenozoic deposits and the isostatic residual gravity over basement, *in* Singer, D.A., ed., An Analysis of Nevada's Metal-Bearing Mineral Resources: Nevada Bureau of Mines and Geology Open-File Report 96-2, p. 2-1–2-10, 1 sheet, http://www.nbmg.unr.edu/dox/ofr962/c2.pdf.

Johnson, R.C., Finn, T.M., and Nuccio, V.F., 2001, Potential for a Basin-Centered Gas Accumulation in the Albuquerque Basin, New Mexico: U.S. Geological Survey Bulletin 2184-C, 21 p.

Jurdy, D.M., and Brocher, T.M., 1980, Shallow velocity model of the Rio Grande rift near Socorro, New Mexico: Geology, v. 8, p. 185–189, doi:10.1130/0091-7613(1980)8<185:SVMOTR>2.0.CO;2.

Karlstrom, K.E., Cather, S.S., Kelley, S.A., Heizler, M.T., Pazzaglia, F.J., and Roy, M., 1999, Sandia Mountains and Rio Grande rift: Ancestry of structures (Proterozoic to Laramide) and history of deformation, *in* Pazzaglia, F.J., and Lucas, S.G., eds., Albuquerque Geology: New Mexico Geological Society Guidebook 50, p. 155–166.

Karlstrom, K.E., Amato, J.M., Williams, M.L., Heizler, M.T., Shaw, C.A., Read, A.S., and Bauer, P.W., 2004, Proterozoic tectonic evolution of the New Mexico region: A synthesis, *in* Mack, G.H., and Giles, K.A., eds., The Geology of New Mexico, A Geologic History: New Mexico Geological Society Special Publication 11, p. 1–34.

Keller, G.R., and Baldridge, W.S., 1999, The Rio Grande rift: A geological and geophysical overview: Rocky Mountain Geology, v. 34, p. 121–130, doi:10.2113/34.1.121.

Keller, G.R., Cordell, L., Davis, G.H., Peeples, W.J., and White, G., 1984, A geophysical study of the San Luis Basin, *in* Baldridge, W.S., Dickerson, P.W., Riecker, R.E., and Zidek, J., eds., Rio Grande Rift: Northern New Mexico: New Mexico Geological Society Guidebook 35, p. 51–57.

Kelley, S.A., Chapin, C.E., and Corrigan, J., 1992, Late Mesozoic to Cenozoic Cooling Histories of the Flanks of the Northern and Central Rio Grande Rift, Colorado and New Mexico: New Mexico Bureau of Mines and Mineral Resources Bulletin 145, 39 p.

Kelley, S.A., Kempter, K.A., McIntosh, W.C., Maldonado, F., Smith, G.A., Connell, S.D., Koning, D.J., and Whiteis, J., 2013, this volume, Syndepositional deformation and provenance of Oligocene to Lower Miocene sedimentary rocks along the western margin of the Rio Grande rift, Jemez Mountains, New Mexico, *in* Hudson, M.R., and Grauch, V.J.S., eds., New Perspectives on Rio Grande Rift Basins: From Tectonics to Groundwater: Geological Society of America Special Paper 494, doi:10.1130/2013.2494(05).

Kelley, V.C., 1977, Geology of Albuquerque Basin, New Mexico: New Mexico Bureau of Mines and Mineral Resources Memoir 33, 59 p., 1 pl.

Kelley, V.C., 1978, Geology of Española Basin, New Mexico: New Mexico Bureau of Mines and Mineral Resources Geologic Map 48, 1 pl.

Kelley, V.C., 1979, Tectonics, Middle Rio Grande rift, New Mexico, *in* Riecker, R.E., ed., Rio Grande Rift—Tectonics and Magmatism: Washington, D.C., American Geophysical Union, p. 57–70.

Kelley, V.C., 1982, Diverse geology of the Hubbell bench, Albuquerque basin, New Mexico, *in* Grambling, J.A., Wells, S.G., and Callender, J.F., eds., Albuquerque Country II: New Mexico Geological Society Guidebook 33, p. 159–160.

Kelley, V.C., and Kudo, A.M., 1978, Volcanoes and Related Basalts of Albuquerque Basin, New Mexico: New Mexico Bureau of Mines and Mineral Resources Circular 156, 30 p.

Kelley, V.C., and Northrop, S.A., 1975, Geology of Sandia Mountains and Vicinity, New Mexico: New Mexico Bureau of Mines and Mineral Resources Memoir 29, 136 p.

Kelley, V.C., and Wood, G.H., 1946, Lucero Uplift, Valencia, Socorro, and Bernalillo Counties, New Mexico: U.S. Geological Survey Oil and Gas Investigations Map OM-47, scale 1:63,360.

Kellogg, K.S., 1999, Neogene basins of the northern Rio Grande rift: Partitioning and asymmetry inherited from Laramide and older uplifts: Tectonophysics, v. 305, p. 141–152, doi:10.1016/S0040-1951(99)00013-X.

Kucks, R.P., Hill, P.L., and Heywood, C.E., 2001, New Mexico Aeromagnetic and Gravity Maps and Data: A Web Site for Distribution of Data: U.S. Geological Survey Open-File Report 01-0061, version 1.0, http://pubs.usgs.gov/of/2001/ofr-01-0061/ (accessed 2002).

Lambiase, J.J., and Bosworth, W., 1995, Structural controls on sedimentation in continental rifts, *in* Lambiase, J.J., ed., Hydrocarbon Habitat in Rift Basins: Geological Society of London Special Publication 80, p. 117–144.

Lewis, C.J., and Baldridge, W.S., 1994, Crustal extension in the Rio Grande rift, New Mexico: Half-grabens, accommodation zones, and shoulder uplifts in the Ladron Peak–Sierra Lucero area, *in* Keller, G.R., and Cather, S.M., eds., Basins of the Rio Grande Rift: Structure, Stratigraphy, and Tectonic Setting: Geological Society of America Special Paper 291, p. 135–155.

Lisenbee, A.L., 2013, this volume, Multi-stage Laramide deformation in the area of the southern Santa Fe embayment (Rio Grande rift), north-central New Mexico, *in* Hudson, M.R., and Grauch, V.J.S., eds., New Perspectives on Rio Grande Rift Basins: From Tectonics to Groundwater: Geological Society of America Special Paper 494, doi:10.1130/2013.2494(10).

Lozinsky, R.P., 1988, Stratigraphy, Sedimentology, and Sand Petrology of the Santa Fe Group and Pre–Santa Fe Tertiary Deposits in the Albuquerque Basin, Central New Mexico [Ph.D. thesis]: Socorro, New Mexico Institute of Mining and Technology, 298 p.

Lozinsky, R.P., 1989, Cenozoic basin-fill stratigraphy and depositional history of the Albuquerque basin, central New Mexico, *in* Anderson, O.J., Lucas, S.G., Love, D.W., and Cather, S.M., eds., Southeastern Colorado Plateau: New Mexico Geological Society Guidebook 40, p. 269–272.

Lozinsky, R.P., 1994, Cenozoic stratigraphy, sandstone petrology, and depositional history of the Albuquerque basin, central New Mexico, *in* Keller, G.R., and Cather, S.M., eds., Basins of the Rio Grande Rift: Structure, Stratigraphy, and Tectonic Setting: Geological Society of America Special Paper 291, p. 73–82.

Lozinsky, R.P., and Tedford, R.H., 1991, Geology and Paleontology of the Santa Fe Group, Southwestern Albuquerque Basin, Valencia County, New Mexico: New Mexico Bureau of Mines and Mineral Resources Bulletin 132, 35 p.

Machette, M.N., 1978, Geologic Map of the San Acacia Quadrangle, Socorro County, New Mexico: U.S. Geological Survey Geologic Quadrangle Map GQ-1415, scale 1:24,000.

Machette, M.N., 1985, Calcic soils of the southwestern United States, *in* Weide, D.L., and Faber, M.L., eds., Soils and Quaternary Geology of the Southwestern United States: Geological Society of America Special Paper 203, p. 1–21.

Machette, M.N., 1998, Contrasts between short- and long-term records of seismicity in the Rio Grande rift—Important implications for seismic hazard assessments in areas of slow extension, *in* Lund, W.R., ed., Western States Seismic Policy Council Proceedings Volume, Basin and Range Province Seismic Hazards Summit: Utah Geological Survey Miscellaneous Publication 98-2, p. 84–95.

Mack, G.H., Seager, W.R., Leeder, M.R., Parea-Arlucea, M., and Salyards, S.L., 2006, Pliocene and Quaternary history of the Rio Grande, the axial river of the southern Rio Grande rift, New Mexico, USA: Earth-Science Reviews, v. 79, p. 141–162, doi:10.1016/j.earscirev.2006.07.002.

Maldonado, F., Connell, S.D., Love, D.W., Grauch, V.J.S., Slate, J.L., McIntosh, W.C., Jackson, P.B., and Byers, F.M., Jr., 1999, Neogene geology of the Isleta Reservation and vicinity, Albuquerque basin, central New Mexico, *in* Pazzaglia, F.J., and Lucas, S.G., eds., Albuquerque Geology: New Mexico Geological Society Guidebook 50, p. 175–188.

Maldonado, F., Slate, J.L., Love, D.W., Connell, S.D., Cole, J.C., and Karlstrom, K.E., 2007, Geologic Map of the Pueblo of Isleta Tribal Lands and Vicinity, Bernalillo, Torrance, and Valencia Counties, Central New Mexico: U.S. Geological Survey Scientific Investigations Map 2913, 1:50,000.

May, S.J., and Russell, L.R., 1994, Thickness of the syn-rift Santa Fe Group in the Albuquerque Basin and its relation to structural style, *in* Keller, G.R., and Cather, S.M., eds., Basins of the Rio Grande Rift: Structure, Stratigraphy, and Tectonic Setting: Geological Society of America Special Paper 291, p. 113–123.

May, S.J., Kelley, S.A., and Russell, L.R., 1994, Footwall unloading and rift shoulder uplifts in the Albuquerque Basin: Their relation to syn-rift fanglomerates and apatite fission-track ages, *in* Keller, G.R., and Cather, S.M., eds., Basins of the Rio Grande Rift: Structure, Stratigraphy, and Tectonic Setting: Geological Society of America Special Paper 291, p. 125–134.

Minor, S.A., ed., 2006, The Cerrillos Uplift, the La Bajada Constriction, and Hydrogeologic Framework of the Santo Domingo Basin, Rio Grande Rift, New Mexico: U.S. Geological Survey Professional Paper 1720, 189 p.

Minor, S.A., Hudson, M.R., Grauch, V.J.S., and Sawyer, D.A., 2006, Structure of the Santo Domingo basin and La Bajada constriction area, New Mexico, *in* Minor, S.A., ed., The Cerrillos Uplift, the La Bajada Constriction, and Hydrogeologic Framework of the Santo Domingo Basin, Rio Grande Rift, New Mexico: U.S. Geological Survey Professional Paper 1720-E, p. 91–115.

Minor, S.A., Hudson, M.R., Caine, J.S., and Thompson, R.A., 2013, this volume, Oblique transfer of extensional strain between basins of the middle Rio Grande rift, New Mexico: Fault kinematic and paleostress constraints, *in* Hudson, M.R., and Grauch, V.J.S., eds., New Perspectives on Rio Grande Rift Basins: From Tectonics to Groundwater: Geological Society of America Special Paper 494, doi:10.1130/2013.2494(14).

Morley, C.K., 1999, Patterns of displacement along large normal faults: Implications for basin evolution and fault propagation, based on examples from East Africa: American Association of Petroleum Geologists Bulletin, v. 83, p. 613–634.

Morley, C.K., 2002, Evolution of large normal faults: Evidence from seismic reflection data: American Association of Petroleum Geologists Bulletin, v. 86, p. 961–978.

Morley, C.K., Harper, R.M., and Wigger, S.T., 1999a, Tectonic inversion in East Africa, *in* Morley, C.K., ed., Geoscience of Rift Systems—Evolution of East Africa: American Association of Petroleum Geologists Studies in Geology 44, p. 193–210.

Morley, C.K., Day, R.A., Lauck, R., Bosher, R., Stone, D.M., Wigger, S.T., Wescott, W.A., Haun, D., Bassett, N., and Bosworth, W., 1999b, Geology and geophysics of the Anza Graben, *in* Morley, C.K., ed., Geoscience of Rift Systems—Evolution of East Africa: American Association of Petroleum Geologists Studies in Geology 44, p. 67–90.

Nabighian, M.N., Ander, M.E., Grauch, V.J.S., Hansen, R.O., LaFehr, T.R., Li, Y., Pearson, W.C., Peirce, J.W., Phillips, J.D., and Ruder, M.E., 2005, The historical development of the gravity method in exploration: Geophysics, v. 70, p. 63ND–89ND.

New Mexico Bureau of Geology and Mineral Resources, 2003, Geologic Map of New Mexico: Socorro, New Mexico Bureau of Geology and Mineral Resources, scale 1:500,000.

Olig, S.S., Eppes, M.C., Forman, S.L., Love, D.W., and Allen, B.D., 2011, Late Quaternary earthquakes on the Hubbell Spring fault system, New Mexico, USA: Evidence for noncharacteristic ruptures of intrabasin faults in the Rio Grande rift, *in* Audemard M., F.A., Michetti, A.M., and McCalpin, J., eds., Geological Criteria for Evaluating Seismicity Revisited: Forty Years of Paleoseismic Investigations and the Natural Record of Past Earthquakes: Geological Society of America Special Paper 479, p. 47–77, doi:10.1130/2011.2479(02).

Parker, R.L., 1973, The rapid calculation of potential anomalies: Geophysical Journal of the Royal Astronomical Society, v. 31, p. 447–455, doi:10.1111/j.1365-246X.1973.tb06513.x.

Pazzaglia, F.J., Woodward, L.A., Lucas, S.G., Anderson, O.J., Wegmann, K.W., and Estep, J.W., 1999, Phanerozoic geologic evolution of the Albuquerque area, *in* Pazzaglia, F.J., and Lucas, S.G., eds., Albuquerque Geology: New Mexico Geological Society Guidebook 50, p. 97–114.

Personius, S.F., and Mahan, S.A., 2003, Paleoearthquakes and eolian-dominated fault sedimentation along the Hubbell Spring fault zone near Albuquerque, New Mexico: Bulletin of the Seismological Society of America, v. 93, p. 1355–1369, doi:10.1785/0120020031.

Peterson, C., and Roy, M., 2005, Gravity and flexure models of the San Luis, Albuquerque, and Tularosa basins in the Rio Grande rift, New Mexico and southern Colorado, *in* Lucas, S.G., Zeigler, K.E., Lueth, V.W., and Owen, D.E., eds., Geology of the Chama Basin: New Mexico Geological Society Guidebook 56, p. 105–114.

Rodriguez, B.D., and Sawyer, D.A., 2013, this volume, Geophysical constraints on Rio Grande rift structure and stratigraphy from magnetotelluric models and borehole resistivity logs, northern New Mexico, *in* Hudson, M.R., and Grauch, V.J.S., eds., New Perspectives on Rio Grande Rift Basins: From Tectonics to Groundwater: Geological Society of America Special Paper 494, doi:10.1130/2013.2494(13).

Rosendahl, B.R., 1987, Architecture of continental rifts with special reference to East Africa: Annual Review of Earth and Planetary Sciences, v. 15, p. 445–503, doi:10.1146/annurev.ea.15.050187.002305.

Roy, M., Karlstrom, K.E., Kelley, S., Pazzaglia, F.J., and Cather, S., 1999, Topographic setting of the Rio Grande rift, New Mexico: Assessing the role of flexural "rift-flank uplift" in the Sandia Mountains, *in* Pazzaglia, F.J., and Lucas, S.G., eds., Albuquerque Geology: New Mexico Geological Society Guidebook 50, p. 167–174.

Russell, L.R., and Snelson, S., 1990, Structural style and tectonic evolution of the Albuquerque Basin segment of the Rio Grande rift, *in* Pinet, B., and Bois, C., eds., The Potential of Deep Seismic Profiling for Hydrocarbon Exploration: Paris, Éditions Technip, p. 175–207.

Russell, L.R., and Snelson, S., 1994a, Structure and tectonics of the Albuquerque Basin segment of the Rio Grande rift: Insights from reflection seismic data, *in* Keller, G.R., and Cather, S.M., eds., Basins of the Rio Grande Rift: Structure, Stratigraphy, and Tectonic Setting: Geological Society of America Special Paper 291, p. 83–112.

Russell, L.R., and Snelson, S., 1994b, Structural style and tectonic evolution of the Albuquerque basin segment of the Rio Grande rift, New Mexico, U.S.A., *in* Landon, S.M., ed., Interior Rift Basins: American Association of Petroleum Geologists Memoir 59, p. 205–258.

Saltus, R.W., and Jachens, R.C., 1995, Gravity and Basin-Depth Maps of the Basin and Range Province, Western United States: U.S. Geological Survey Geophysical Investigations Map GP-1012, scale 1:2,500,000.

Schlische, R.W., 1995, Geometry and origin of fault-related folds in extensional settings: American Association of Petroleum Geologists Bulletin, v. 79, p. 1661–1678.

Schlische, R.W., and Anders, M.H., 1996, Stratigraphic effects and tectonic implications of the growth of normal faults and extensional basins, *in* Beratan, K.K., ed., Reconstructing the History of Basin and Range Extension Using Sedimentology and Stratigraphy: Geological Society of America Special Publication 303, p. 183–203.

Schlische, R.W., and Withjack, M.O., 2008, Origin of fault domains and fault-domain boundaries (transfer zones and accommodation zones) in extensional provinces: Result of random nucleation and self-organized fault growth: Journal of Structural Geology, v. 31, p. 910–925, doi:10.1016/j.jsg.2008.09.005.

Shroba, R.R., Thompson, R.A., Schmidt, D.L., Personius, S.F., Maldonado, F., and Brandt, T.R., 2003, Geologic Map of the La Mesita Negra SE Quadrangle, Bernalillo County, New Mexico: U.S. Geological Survey Miscellaneous Field Studies Map MF-2416, scale 1:24,000.

Simpson, R.W., Jachens, R.C., Blakely, R.J., and Saltus, R.W., 1986, A new isostatic map of the conterminous U.S. with a discussion on the significance of isostatic residual anomalies: Journal of Geophysical Research, v. 91, p. 8348–8372, doi:10.1029/JB091iB08p08348.

Smith, G.A., McIntosh, W., and Kuhle, A.J., 2001, Sedimentologic and geomorphic evidence for seesaw subsidence of the Santo Domingo accommodation-zone basin, Rio Grande rift, New Mexico: Geological Society of America Bulletin, v. 113, p. 561–574, doi:10.1130/0016-7606(2001)113<0561:SAGEFS>2.0.CO;2.

Spiegel, Z., and Baldwin, B., 1963, Geology and Water Resources of the Santa Fe Area, New Mexico; with Contributions by F.E. Kottlowski and E.L. Barrows and a Section on Geophysics by H.A. Winkler: U.S. Geological Survey Water-Supply Paper 1525, 258 p.

Stewart, J.H., Anderson, R.E., Aranda-Gómez, J.J., Beard, L.S., Billingsley, G.H., Cather, S.M., Dilles, J.H., Dokka, R.K., Faulds, J.E., Ferrari, L., Grose, T.L.T., Henry, C.D., Janecke, S.U., Miller, D.M., Richard, S.M., Rowley, P.D., Roldán-Quintana, J., Scott, R.B., Sears, J.W., and Williams, V.S., 1998, Map showing Cenozoic tilt domains and associated structural features, western North America, *in* Faulds, J.E., and Stewart, J.H., eds., Accommodation Zones and Transfer Zones: The Regional Segmentation of the Basin and Range Province: Geological Society of America Special Paper 323, plate 1, scale 1:5,000,000.

Tedford, R.H., and Barghoorn, S., 1999, Santa Fe Group (Neogene), Ceja del Rio Puerco, northwestern Albuquerque Basin, Sandoval County, New Mexico, *in* Pazzaglia, F.J., and Lucas, S.G., eds., Albuquerque Geology: New Mexico Geological Society Guidebook, v. 50, p. 327–335.

Wernicke, B.P., and Axen, G.J., 1988, On the role of isostasy in the evolution of normal fault systems: Geology, v. 16, p. 848–851.

Wong, I., Olig, S., Dober, M., Silva, W., Wright, D., Thomas, P., Gregor, N., Sanford, A., Lin, K.-W., and Love, D., 2004, Earthquake scenario and probabilistic ground-shaking hazard maps for the Albuquerque–Belen–Santa Fe, New Mexico, corridor: New Mexico Geology, v. 26, p. 3–33.

Woodward, L.A., 1977, Rate of crustal extension across the Rio Grande Rift near Albuquerque, New Mexico: Geology, v. 5, p. 269–272, doi:10.1130/0091-7613(1977)5<269:ROCEAT>2.0.CO;2.

Wu, Z., 1986, Shallow structure of the southern Albuquerque basin (Rio Grande rift), New Mexico, from COCORP seismic reflection data, *in* Barazangi, M., and Brown, L.D., eds., Reflection Seismology: The Continental Crust: American Geophysical Union Geodynamics Series, v. 14, p. 293–304.

Younes, A.I., and McClay, K., 2002, Development of accommodation zones in the Gulf of Suez–Red Sea rift, Egypt: American Association of Petroleum Geologists Bulletin, v. 86, p. 1003–1026.

Manuscript Accepted by the Society 20 July 2012

Printed in the USA